Serb. Astron. J. № 183 (2011), 37 - 61 **UDC 524.6–54 : 524.3–52–54**
DOI: 10.2298/SAJ1183037C Original scientific paper

A SIMPLE MULTISTAGE CLOSED-(BOX+RESERVOIR) MODEL OF CHEMICAL EVOLUTION

R. Caimmi
E–mail: *roberto.caimmi@unipd.it*

Dipartimento di Astronomia, Università di Padova
Vicolo Osservatorio 3/2, I-35122 Padova, Italy

(Received: October 21, 2010; Accepted: November 10, 2011)

SUMMARY: Simple closed-box (CB) models of chemical evolution are extended on two respects, namely (i) simple closed-(box+reservoir) (CBR) models allowing gas outflow from the box into the reservoir (Hartwick 1976) or gas inflow into the box from the reservoir (Caimmi 2007) with rate proportional to the star formation rate, and (ii) simple multistage closed-(box+reservoir) (MCBR) models allowing different stages of evolution characterized by different inflow or outflow rates. The theoretical differential oxygen abundance distribution (TDOD) predicted by the model maintains close to a continuous broken straight line. An application is made where a fictitious sample is built up from two distinct samples of halo stars and taken as representative of the inner Galactic halo. The related empirical differential oxygen abundance distribution (EDOD) is represented, to an acceptable extent, as a continuous broken line for two viable [O/H]-[Fe/H] empirical relations. The slopes and the intercepts of the regression lines are determined, and then used as input parameters to MCBR models. Within the errors $(\mp\sigma)$, regression line slopes correspond to a large inflow during the earlier stage of evolution and to low or moderate outflow during the subsequent stages. A possible inner halo - outer (metal-poor) bulge connection is also briefly discussed. Quantitative results cannot be considered for applications to the inner Galactic halo, unless selection effects and disk contamination are removed from halo samples, and discrepancies between different oxygen abundance determination methods are explained.

Key words. galaxies: evolution – stars: formation – stars: evolution

1. INTRODUCTION

The empirical metallicity distributions of long-lived stars of different populations, constrain models for formation and evolution of the Galaxy. Simple closed-box (CB) models make a useful tool in the description of galactic chemical evolution. The original formulation (Searle and Sargent 1972, Pagel and Patchett 1975) relies on instantaneous recycling and homogeneous mixing approximations i.e. gas from dying stars is instantaneously returned to and homogeneously mixed with the interstellar medium.

The existence of a G-dwarf problem i.e. detection of too few metal deficient G dwarf (or, more generally, of a selected spectral type) with respect to that which could be expected from simple CB models of chemical evolution (e.g. Searle and Sargent 1972, Pagel and Patchett 1975, Haywood 2001) was first established in the solar neighbourhood (van den Bergh 1962, Schmidt 1963). Although in a less extreme form, a G-dwarf problem appears to exist both in the halo (e.g. Hartwick 1976, hereafter quoted as H76, Prantzos 2003) and in the bulge (e.g. Fer-

reras et al. 2003). In addition, a G-dwarf problem has been recognized in both bulge-dominated and disk-dominated galaxies (Henry and Worthey 1999), which is consistent with the idea that the G-dwarf problem is universal (Worthey et al. 1996).

According to current ΛCDM cosmological scenarios, galaxies were largely built out of disrupted smaller subunits (dSph galaxies whose surviving cores could be massive globular clusters). A similar process is presently occurring on a larger scale: a central bulge (a cD galaxy) is accreting in galaxy clusters, at the expense of infalling smaller galaxies. Recent literature suggests that the assembly through mergers is only true for massive systems and bulges while low-mass galaxies were mostly built by smooth accretion of intergalactic and halo gas (e.g. Keres et al. 2005, Guo and White 2008). In this view, a universal G-dwarf problem appears to be closely related to the initial very rapid gas inflow related to low-mass early galaxies or systems (Milky Way included).

With regard to the Galaxy, the empirical differential oxygen abundance distribution (EDOD) shows that (i) at least two different stages of (chemical) evolution exist, and (ii) each stage can be described using an extended simple CB model, for both the inner halo (Caimmi 2007, hereafter quoted as C07), the bulge (C07), the thick disk (Caimmi and Milanese 2009, hereafter quoted as CM09), and the thin disk (CM09). In particular, the earlier stage is marked by an initially increasing EDOD. Understanding different stages of Galactic (or sub-Galactic) chemical evolution can be used to get further insight on the evolution of important global properties of stellar and gaseous components of galaxies.

The advantage of the EDOD, $\psi = \log[\Delta N/(N\Delta\phi)]$[1], on the oxygen abundance distribution, $\Psi = \Delta N/N$, is that the theoretical differential oxygen abundance distribution (TDOD) predicted by extended simple CB models is a straight line on the $(\mathsf{O}\phi\psi)$ plane, which provides a more sensitive test (Pagel 1989, Malinie et al. 1993, Rocha-Pinto and Maciel 1996, Caimmi 2000 + erratum 2001a, hereafter quoted together as C00, Caimmi 2001b, hereafter quoted as C01, C07, Caimmi 2008, CM09).

Simple CB models of chemical evolution were first extended allowing for gas outflow (H76) and later for moderate gas inflow, with same metal abundance as in the pre existing gas, yielding negative TDOD slopes in the $(\mathsf{O}\phi\psi)$ plane. On the other hand, the low-metallicity tail of the EDOD is fitted to a straight line with positive slope for both the halo (C07), the bulge (C07), the thick disk (CM09), and the thin disk (CM09), which is achieved by extending simple CB models to strong gas inflow with metal abundance nearly equal to the one in the pre-exisiting gas.

In this view, different stages of evolution are related to different domains in the normalized oxygen abundance, $(\phi_{\rm U})_i \leq \phi \leq (\phi_{\rm U})_f$, where the EDOD is fitted to a regression line, $\psi = a_{\rm U}\phi + b_{\rm U}$, with slope, $a_{\rm U}$, and intercept, $b_{\rm U}$ (U = I, II, ..., is the stage considered, beginning and ending at i and f configurations, respectively). For reasons of continuity, the final values of parameters related to a selected stage must necessarily coincide with the corresponding initial values related to the next stage, with the exception of the outflow or inflow rate, which can be deduced from the EDOD, and related oxygen abundance, which must be assigned but has little influence on the TDOD. Accordingly, the knowledge of present values allows the calculation of past values, in the light of the model, getting insight on the formation and evolution of the system under consideration.

In summary, the current paper is aimed to the following main points: (i) metallicity distribution related to a fictitious sample (hereafter quoted as the fs10 sample), supposed to be representative of the inner Galactic halo (Subsection 2.1); (ii) choice of two different [O/H]-[Fe/H] empirical relations deduced from recent samples (RB09, Fal09, Sal09) (Subsection 2.2); (iii) EDOD determination from the fs10 sample by use of the above mentioned [O/H]-[Fe/H] empirical relations (Subsection 2.3); (iv) formulation of extended simple CB models, namely (a) simple CBR models, allowing for gas outflow or inflow, and (b) simple MCBR models, allowing for different stages of evolution (Subsections 3.1, 3.2 and 3.4); (v) determination of the best fitting TDOD to the EDOD inferred from the fs10 sample (Subsection 3.3); (vi) application to a special stellar system resembling the inner Galactic halo (Subsections 3.5 and 3.6). In addition, the discussion and the conclusion make the subject of Subsection 3.7 and Section 4, respectively. Further details are specified in the Appendix.

2. DATA AND INFERRED QUANTITIES

According to several investigations on both globular clusters (e.g. Salaris and Weiss 2002, De Angeli et al. 2005, Marin-Franch et al. 2009) and field halo stars (e.g. Schuster et al. 2006, Carollo et al. 2007, 2010, Nissen and Schuster 2010), one part of the Galactic halo (inner halo) was formed via rapid relaxation of a non virialized gaseous subsystem, whereas the other part (outer halo) was formed slowly and chaotically via accretion of fragments or satellites. For further details refer to a recent attempt (Jofré and Weiss 2011).

The inner halo population dominates within about 15 pc along the Galactic plane and about 10 pc in height, showing a metallicity peak at [Fe/H] ≈ -1.6, while the outer halo population extends well outside where a metallicity peak occurs at [Fe/H] ≈ -2.2 (Carollo et al. 2007, 2010). The existence of a

[1]Caption of symbols: $\phi = Z_{\rm O}/(Z_{\rm O})_\odot$ is the oxygen abundance normalized to the solar value, N is the population of the sample under consideration, and ΔN is the number of sample objects within a bin centered in ϕ and bounded at $\phi \mp \Delta\phi/2$.

clear net retrograde rotation for the outer halo population has recently been doubted as ascribed to biases in distance estimates (Schönrich et al. 2011). From this point on, attention shall be focused on the inner halo population.

The following ingredients are necessary for determination of the EDOD (in particular, related to the inner halo), from which input parameters of a selected model are deduced: (i) a representative sample; (ii) a related [Fe/H] distribution; (iii) a [O/H]-[Fe/H] empirical relation. Each point will be separately dealt within the forthcoming subsections.

2.1. Building up a fictitious sample (fs10)

In building up a fictitious sample (the fs10 sample) of inner halo stars, two different samples will be considered, namely the RN91 sample ($N = 372$) of kinematically selected halo subdwarfs (Ryan and Norris 1991, hereafter quoted as RN91) and the H V sample ($N = 3439$) of metal-poor stars selected from the Hamburg/ESO objective prism survey. More specifically, the H V sample has been determined from a subsample ($N = 1638$) with available spectroscopic follow-up observations, by means of scaling to the full parent sample ($N = 3439$). For further details refer to the parent paper (Schörck et al. 2009, hereafter quoted as H V).

The RN91 sample can be considered complete within the range $-3.4 < [\mathrm{Fe/H}] < -1.0$ even if substantial uncertainty is expected at the lower tail $-3.4 < [\mathrm{Fe/H}] < -3.0$ due to poorly populated bins (two stars per bin). At different abundance the sample is incomplete and suffers contamination from disk stars at the high-metallicity tail $[\mathrm{Fe/H}] \geq -1.0$. Sample stars are crossing the solar neighbourhood.

The H V sample can be considered as complete within the range $-4.2 < [\mathrm{Fe/H}] < -2.8$. At different abundance the sample is incomplete and suffers both selection effects ($[\mathrm{Fe/H}] > -2.8$) and contamination from disk stars ($[\mathrm{Fe/H}] > -2.0$). The sample is dominated by stars at distances of less than about 5 kpc from the Sun, even if a few objects exceed distances of up to 50 kpc.

The H V sample is mainly made of giant stars. A subsequent study on the stellar content of the Hamburg/ESO survey has been focused on a sample ($N = 617$) of main sequence turnoff stars (Li et al. 2010). Both samples exhibit a quite analogous metal abundance distribution where the halo population dominates ($[\mathrm{Fe/H}] < -2.0$), while the contrary holds for higher values ($[\mathrm{Fe/H}] > -2.0$). In the latter case, the H V sample is also affected by the survey-volume effect. For further details refer to the parent paper (Li et al. 2010).

Basing on the above considerations, the following working hypotheses are made.

(1) The H V sample ($N = 3439$) is representative of the inner halo within the range $-4.2 < [\mathrm{Fe/H}] < -2.8$ where selection effects are minimized and contamination from disk stars is negligible (H V).

(2) The RN91 sample ($N = 372$) is representative of the inner halo within the range $-3.0 < [\mathrm{Fe/H}] < +0.2$ with a caveat due to contamination from disk stars for $[\mathrm{Fe/H}] > -1.0$ (RN91).

(3) The RN91 and H V sample are equally representative (even if belonging to different populations) of the inner halo within the range $-3.0 \leq [\mathrm{Fe/H}] \leq -2.8$ where the number of stars is $(\Delta N)_{\mathrm{RN91}} = 8$ and $(\Delta N)_{\mathrm{H\,V}} = 160$, respectively.

Accordingly, the fs10 sample can be built up from the RN91 and H V samples, by normalizing to the same number of stars within the metallicity range where the above mentioned samples are supposed to be equally representative of the inner halo. More specifically, the normalization shall be performed with respect to the H V sample, but the Poissonian error related to each bin shall remain unchanged with respect to the parent sample, with the minimum among the two retained for the bin where the parent samples are equally representative of the inner halo. Then the number of stars belonging to the fs10 sample, with regard to a selected metallicity bin, remains unchanged or is multiplied by a factor 20 depending whether the parent sample is H V ($[\mathrm{Fe/H}] \leq -2.8$) or RN91 ($[\mathrm{Fe/H}] > -2.8$), respectively, yielding a fictitious population $N = 7452$.

Due to the presence of only two stars in each bin centered on $[\mathrm{Fe/H}] = -3.1, -3.3$, respectively, involving larger errors with regard to RN91 sample, the normalization has not been performed on a wider range $-3.4 \leq [\mathrm{Fe/H}] \leq -2.8$ which would also imply fractional bin population. More specifically, the conversion factor would be 23.2 instead of 20, but adding an extra star to each above mentioned bin containing two stars yields again a conversion factor very close to 20.

2.2. The [O/H]-[Fe/H] empirical relation

In dealing with simple models of chemical evolution, involving the assumption of instantaneous recycling, the predicted metal abundance has to be compared to the observed oxygen (or any other primary element) abundance (e.g. Pagel 1989, C00, C01). Unfortunately, oxygen is more difficult than iron to detect, and an empirical formula may be needed to express the former as a function of the latter. The population of available samples where oxygen abundances are directly determined, does not exceed a few hundreds at most (e.g. Ramirez et al. 2007, Melendez et al. 2008, Rich and Boesgaard 2009, hereafter quoted as RB09, Fabbian et al. 2009, hereafter quoted as Fal09, Schmidt et al. 2009, hereafter quoted as Sal09). With regard to the halo, only the RB09 and Fal09 samples can be considered representative, while the Sal09 sample will be included for comparison, and the remaining above quoted two will be excluded.

The RB09 sample ($N = 49$) is made of a homogeneous subsample ($N = 24$) of metal-poor ($-3.5 < [\mathrm{Fe/H}] < -2.2$) stars, and a non homogeneous subsample ($N = 25$) of higher-metallicity

Table 1. Values of effective temperature $T_{\rm eff}$, decimal logarithm of surface gravity $\log g$, iron abundance [Fe/H], and oxygen abundance [O/H], for $N = 11$ stars in common between the RB09 and Fal09 sample. With regard to the latter, oxygen abundance has been determined using three different methods, LTE, SH0, SH1, respectively, and oxygen abundances related to LP831-070 are upper limits. For further details refer to the text.

star	RN09				Fal09					
	$T_{\rm eff}$	$\log g$	[Fe/H]	[O/H] LTE	$T_{\rm eff}$	$\log g$	[Fe/H]	[O/H] LTE	[O/H] SH0	[O/H] SH1
LP651-04	6030	4.26	−2.89	−2.04	6371	4.20	−2.63	−1.62	−2.21	−1.93
BD-13°3442	6090	4.11	−2.91	−2.15	6366	3.99	−2.69	−1.77	−2.39	−2.11
G11-44	5820	3.58	−2.29	−1.63	6178	4.35	−2.03	−1.29	−1.47	−1.40
G64-12	6074	3.72	−3.45	−2.24	6435	4.26	−3.24	−2.21	−3.10	−2.71
G64-37	6122	3.87	−3.28	−2.32	6432	4.24	−3.08	−2.24	−3.12	−2.70
LP635-14	5932	3.57	−2.71	−2.00	6367	4.11	−2.39	−1.60	−2.03	−1.85
LP815-43	6405	4.37	−2.76	−1.86	6483	4.21	−2.71	−1.95	−2.70	−2.36
HD084937	6206	3.89	−2.20	−1.49	6357	4.07	−2.11	−1.39	−1.64	−1.56
HD140283	5692	3.47	−2.56	−1.72	5849	3.72	−2.38	−1.67	−1.91	−1.81
HD194598	5875	4.20	−1.25	−1.00	6020	4.30	−1.15	−0.51	−0.75	−0.68
LP831-070	5985	4.75	−3.06	−2.45	6232	4.36	−2.93	−2.13	−2.95	−2.54

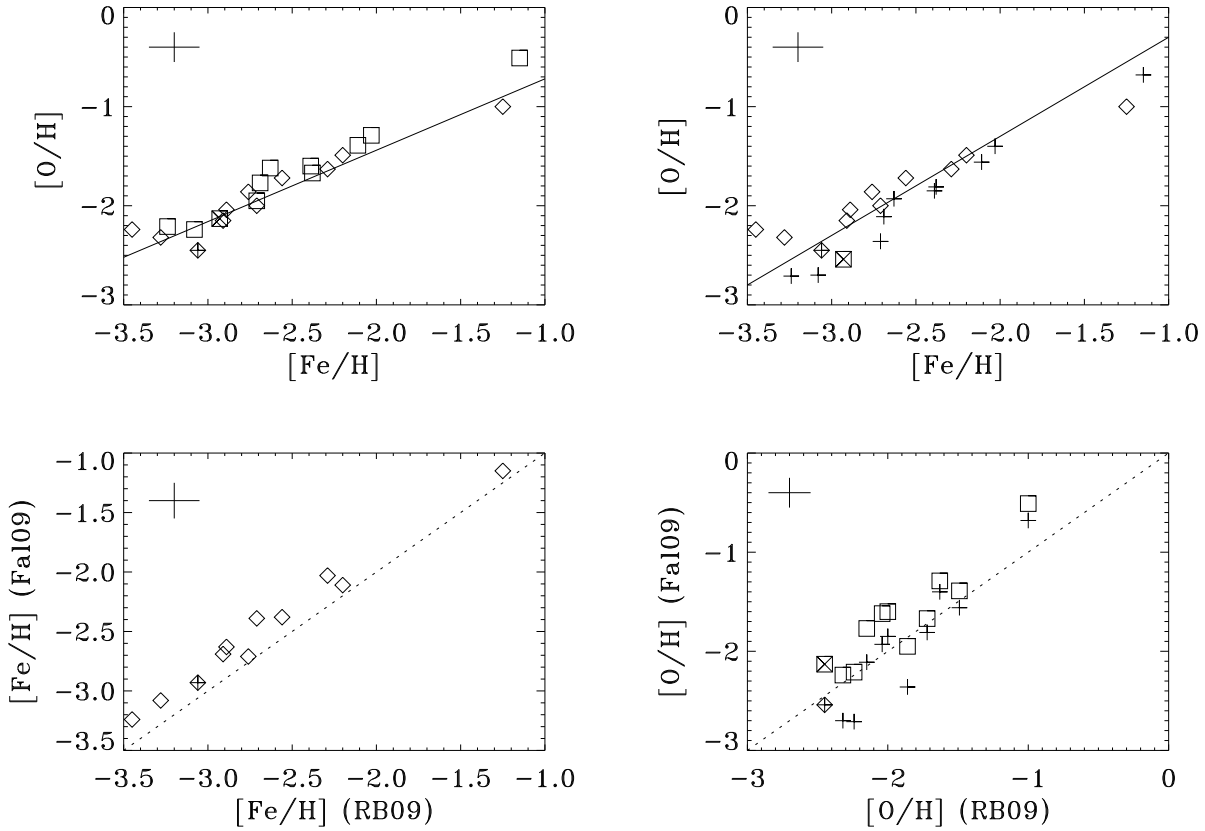

Fig. 1. *Comparison between (i) [O/H]-[Fe/H] empirical relations deduced from 11 halo stars in common among RB09 (upper panels, diamonds) and Fal09, case LTE (top left, squares), case SH1 (top right, crosses), and (ii) [Fe/H] (bottom left) and [O/H] (bottom right), case LTE (squares), case SH1 (crosses), deduced from the above mentioned stars. The composite symbols mark LP831-070, where only an upper limit to oxygen abundance is available in the Fal09 sample. The straight lines in upper panels are [O/H] = 0.72[Fe/H] (left) and [O/H] = [Fe/H] + 0.70 (right). The 1:1 correspondence in lower panels is represented by a dashed line. Typical uncertainties are visualized as crosses on the top left corner of each panel.*

($-3.1 < [Fe/H] < -0.5$) stars. In both cases, the stellar population remains unspecified and oxygen abundance has been determined using standard local thermodynamical equilibrium (LTE) and one-dimensional hydrostatic model atmospheres. The calculated oxygen abundance is independent of the solar value. Typical uncertainties are $\Delta[Fe/H] = \mp 0.15$ and $\Delta[O/H] = \mp 0.15$. Standard deviations are also provided for each star. For further details refer to the parent paper (RB09).

The Fal09 sample ($N = 43$) is made of halo stars ($-3.3 < [Fe/H] < -1.0$) where the oxygen abundance has been determined using three different methods involving (a) LTE one-dimensional hydrostatic model atmospheres; (b) three-dimensional hydrostatic model atmospheres in absence of LTE with no account taken of the inelastic collisions via neutral H atoms ($S_H = 0$), hereafter quoted as SH0; (c) three-dimensional hydrostatic model atmospheres in absence of LTE with due account taken of the inelastic collisions via neutral H atoms ($S_H = 1$), hereafter quoted as SH1. For a single object (LP831-070) only an upper limit to oxygen abundance has been determined. Typical uncertanties are $\Delta[Fe/H] = \mp 0.15$ and $\Delta[O/H] = \mp 0.15$. Standard deviations are not provided for each star. For further details refer to the parent paper (Fal09).

The RB09 and Fal09 samples have $N = 11$ (necessarily halo) stars in common, where the values assumed for effective temperature and surface gravity have been determined using different methods, yielding different values for each star, as shown in Table 1.

A comparison between [O/H]-[Fe/H] empirical relations deduced from data listed in Table 1, in connection with RB09 and Fal09 (case LTE, left; SH1, right) samples, is presented in Fig. 1, upper panels, while the correspondance between [Fe/H] (left) and [O/H] (right), deduced from the above mentioned data, is shown in lower panels.

With regard to Fal09 sample, the case SH0 has not been considered, as it seems to overcorrect LTE abundances and yield values of [O/Fe] which are probably too low. For further details refer to the parent paper (Fal09).

It can be seen that the [O/H]-[Fe/H] empirical relation is slightly affected by the parent sample in the LTE case, with the exception of the most metal-rich sample object (Fig. 1, top left panel). A low discrepancy appears in the SH1 case (Fig. 1, top right panel), where the results in absence of LTE approximation are available for the Fal09 sample only. The occurrence of a systematic difference in [Fe/H] determinations is probably due to different methods

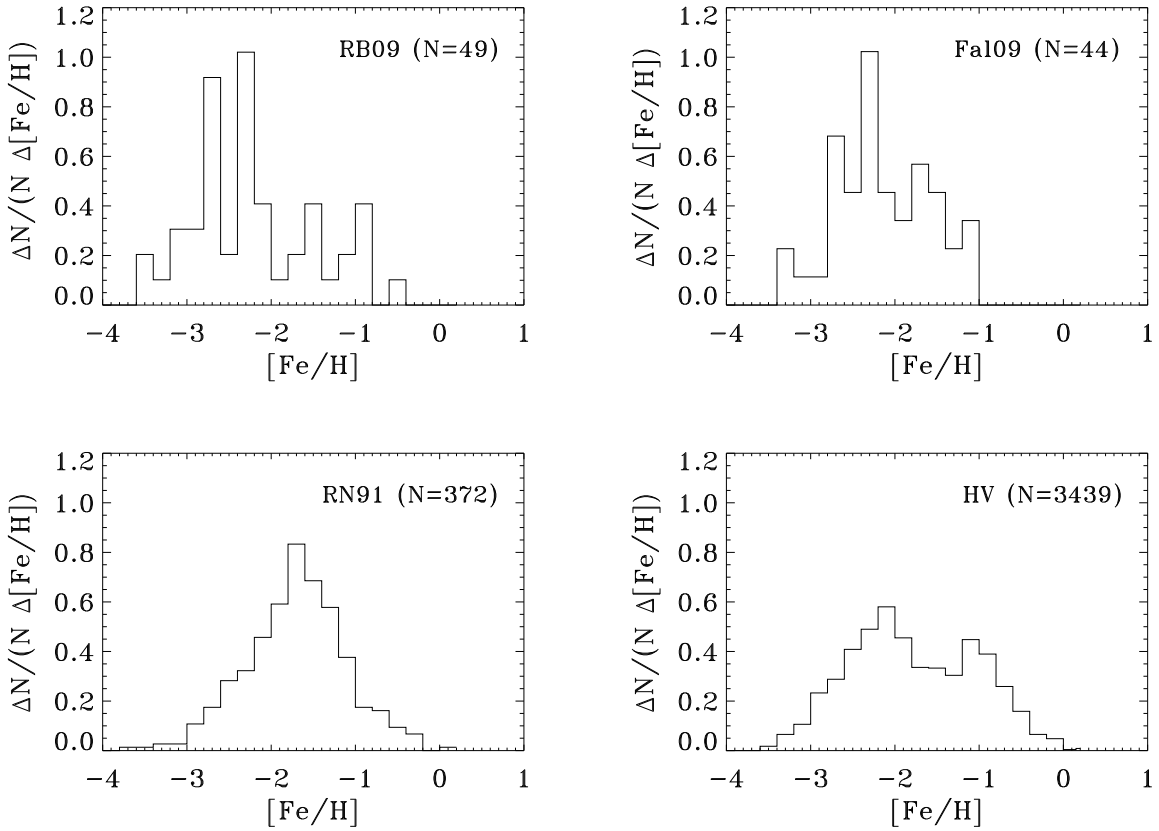

Fig. 2. *[Fe/H] distributions (normalized to the unit area) related to four different samples discussed in the text. Sample denomination and population are indicated in each panel. In all cases, the bin width is* $\Delta[Fe/H] = 0.2$.

related to different samples, which makes all points lie above the straight line with unit slope (Fig. 1, bottom left panel). The same holds, though to a lesser extent, for [O/H] determinations related to the LTE case (Fig. 1, bottom right panel, squares), while points related to the SH1 case (Fig. 1, bottom right panel, crosses) lie both above and below the straight line with unit slope.

The normalized [Fe/H] distributions related to the RB09 and Fal09 sample are plotted in Fig. 2 (upper panels) where a similar trend is shown and, in particular, both exhibit a peak near [Fe/H] = −2.2, similar to their counterpart deduced from the H V sample (bottom right panel) but in contrast with their counterpart deduced from the RN91 sample (bottom left panel).

Then the RB09 and Fal09 samples seem to be representative of the metal-poor halo. Accordingly, the determination of the EDOD from the [Fe/H] distribution related to RN91 and H V samples has to be made under the assumption that the [O/H]-[Fe/H] empirical relations, deduced from the RB09 and Fal09 samples, hold to a similar extent regardless of the metal abundance.

The [O/H]-[Fe/H] empirical relations deduced from RB09, Fal09 (cases LTE, SH0, SH1), and Sal09 samples, shown in Fig. 3, are interpolated using six different regression models.

For heteroscedastic data and homoscedastic models, the typical uncertainties are assigned to all the data points. With regard to the special case of bisector regression, the results are listed in Table 2. A similar trend is shown using different choices, namely classical, inverse, orthogonal, reduced major-axis, and generic regression models (Isobe et al. 1990, Feigelson and Babu 1992, Caimmi 2011a,b).

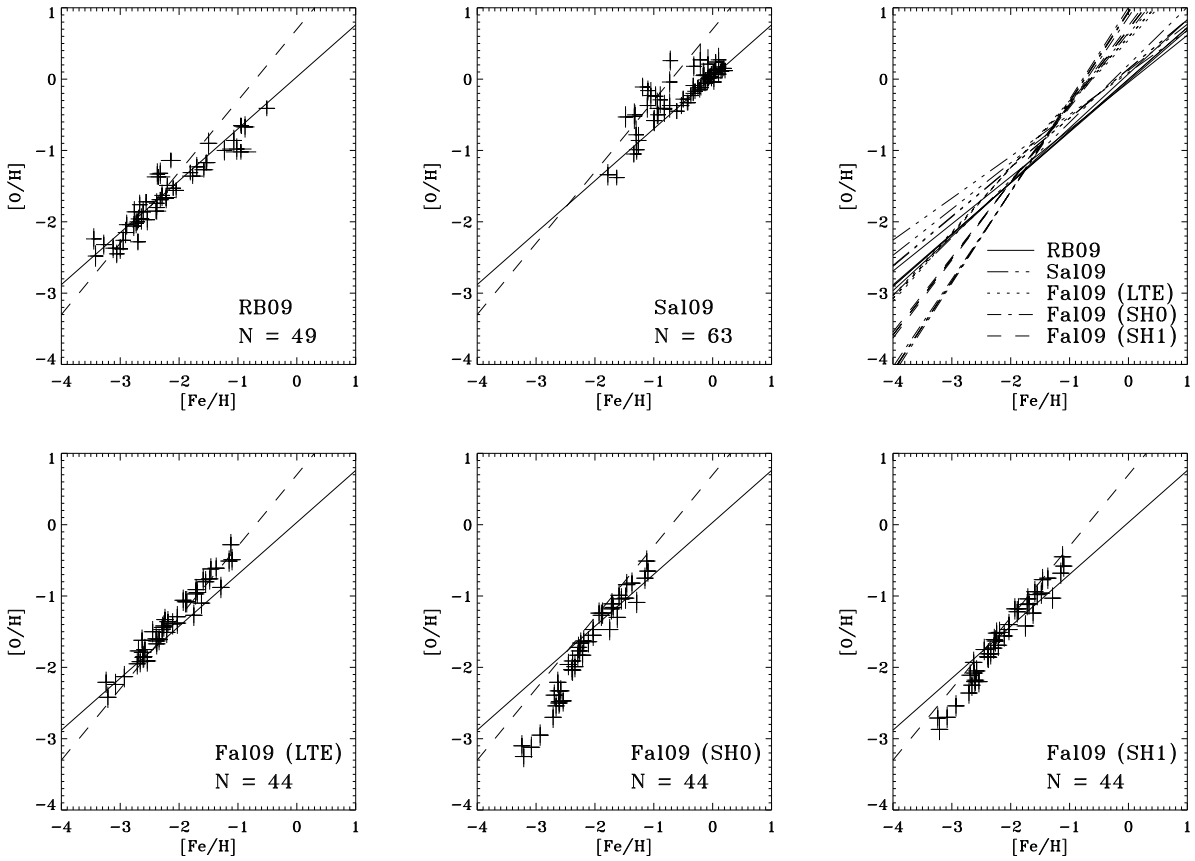

Fig. 3. *The [O/H]-[Fe/H] empirical relation deduced from two samples with heteroscedastic data, RB09 and Sal09, and three samples with homoscedastic data, Fal09, cases LTE, SH0, and SH1, indicated in each panel together with related population. Also plotted in each panel are the adopted linear dependences, [O/H] = 0.72[Fe/H] (full) and [O/H] = [Fe/H] + 0.70 (dashed). The regression lines related to five different methods are shown for each sample in the top right panel. For further details refer to the text.*

Table 2. Regression line slope and intercept estimators $\hat{a}$ and $\hat{b}$ and related dispersion estimators $\hat{\sigma}_{\hat{a}}$ and $\hat{\sigma}_{\hat{b}}$ for bisector regression models applied to the [O/H]-[Fe/H] empirical relation deduced from the samples mentioned in the text.

sample	case	$\hat{a}$	$\hat{\sigma}_{\hat{a}}$	$\hat{b}$	$\hat{\sigma}_{\hat{b}}$
RB09		0.7253	0.0278	−0.0025	0.0665
Sal09		0.6916	0.0513	+0.1431	0.0282
Fal09	LTE	0.9169	0.0310	+0.5916	0.0706
	SH0	1.2568	0.0441	+0.9367	0.0998
	SH1	1.0716	0.0332	+0.6993	0.0760

An inspection of Fig. 3 and Table 2 shows that systematic errors related to different methods and/or different spectral lines in oxygen abundance determination, are dominant on both the dispersion due to measurement errors and intrinsic scatter. At this stage, a precise fit to the data extracted from a selected sample would be meaningless, and only acceptable fits related to different situations will be considered. Accordingly, the following [O/H]-[Fe/H] empirical relations:

$$[\mathrm{O/H}] = 0.72[\mathrm{Fe/H}] \quad , \tag{1}$$

with regard to the RB09 sample, Fig. 3 (full lines on data points), and:

$$[\mathrm{O/H}] = [\mathrm{Fe/H}] + 0.70 \quad , \tag{2}$$

with regard to the Fal09 sample, case SH1, Fig. 3 (dashed lines on data points), will be used for determining the EDOD from the [Fe/H] distribution, related to a selected sample. The regression lines related to the above mentioned methods are shown for each sample in the top right panel of Fig. 3.

2.3. The empirical differential oxygen abundance distribution (EDOD)

With regard to the selected [O/H]-[Fe/H] empirical relation:

$$[\mathrm{O/H}] = a[\mathrm{Fe/H}] + b \quad , \tag{3}$$

and the specified [Fe/H] distribution, let [Fe/H], $[\mathrm{Fe/H}]^{\mp}$, be the coordinates of a selected bin centre and bin left (−) and right (+) extremum, respectively, and [O/H], $[\mathrm{O/H}]^{\mp}$ their counterparts deduced via Eq. (3) for the related [O/H] distribution. Accordingly, the bin semiamplitude reads:

$$\Delta^{\mp}[\mathrm{O/H}] = \frac{[\mathrm{O/H}]^{+} - [\mathrm{O/H}]^{-}}{2} = a\frac{[\mathrm{Fe/H}]^{+} - [\mathrm{Fe/H}]^{-}}{2} = a\Delta^{\mp}[\mathrm{Fe/H}] \quad , \tag{4}$$

where [Fe/H] and [O/H] are logarithmic number abundances normalized to the solar value (e.g. C07).

The oxygen mass abundance normalized to the solar value ϕ to a good extent may be expressed as (e.g. C07):

$$\phi = \frac{Z_{\mathrm{O}}}{(Z_{\mathrm{O}})_{\odot}} = \exp_{10}[\mathrm{O/H}] \quad , \tag{5}$$

and the selected bin centre and bin semiamplitude, related to the [O/H] distribution, read (e.g. C07):

$$\phi = \frac{1}{2}\{\exp_{10}[\mathrm{O/H}]^{+} + \exp_{10}[\mathrm{O/H}]^{-}\} \quad , \tag{6}$$

$$\Delta^{\mp}\phi = \frac{1}{2}\{\exp_{10}[\mathrm{O/H}]^{+} - \exp_{10}[\mathrm{O/H}]^{-}\} \quad , \tag{7}$$

where the bin width is variable for a constant bin width related to the [O/H] distribution.

Following earlier attempts (Rocha-Pinto and Maciel 1996, C00, C01, C07), the EDOD in a selected class of objects is defined as:

$$\psi(\phi) = \log\frac{\Delta N}{N\Delta\phi} \quad , \tag{8}$$

where ΔN is the number of objects within the normalized oxygen abundance bin $\Delta\phi$ centered on ϕ, and N is the number of sample objects. The increment ratio $\Delta N/\Delta\phi$ used in earlier attempts (Pagel 1989, Malinie et al. 1993) is replaced by its normalized counterpart $\Delta N/(N\Delta\phi)$ to allow comparison between different samples. The uncertainty on ΔN is evaluated from Poisson errors (e.g. RN91) as $\sigma_{\Delta N} = (\Delta N)^{1/2}$ and the related uncertainty in the EDOD is:

$$\Delta^{\mp}\psi = |\psi - \psi^{\mp}| = \log\left[1 \mp \frac{(\Delta N)^{1/2}}{\Delta N}\right] \quad , \tag{9a}$$

$$\psi^{\mp} = \log\frac{\Delta N \mp (\Delta N)^{1/2}}{N\Delta\phi} \quad , \tag{9b}$$

where $\psi^{-} \to -\infty$ in the limit $\Delta N \to 1$. For further details refer to the parent papers (C01, C07).

The EDOD related to RN91, H V, and fs10 samples are listed in Table 3 for the [O/H]-[Fe/H] empirical relations expressed by Eqs. (1) and (2), the left and right side, respectively.

The EDOD related to the fs10 sample, taken to be representative of the inner halo, is plotted in Fig. 4 for the [O/H]-[Fe/H] empirical relations expressed by Eqs. (1) and (2), the left and right panel, respectively.

Upper panels represent the whole distribution, while lower panels zoom the low-metallicity range. The vertical bars on the horizontal axis mark [Fe/H] = −2.2, −1.6 where the global [Fe/H] distribution of the outer and inner halo, respectively, peak according to recent results (Carollo et al. 2007, 2010), and [Fe/H] = −0.8, where a transition from halo to bulge/disk globular clusters occurs (Mackey and van den Bergh 2005).

Table 3. The empirical, differential oxygen abundance distribution (EDOD) in the inner halo, deduced from the fs10 sample ($N = 7452$) using two different [O/H]-[Fe/H] empirical relations, determined from interpolation to two different data sets, RB09 in presence of the local thermodynamic equilibrium approximation (left side), and Fal09 in absence of the local thermodynamic equilibrium approximation, case SH1 (right side). The fictitious fs10 sample results from the combination of the H V sample ($N = 3439$) for lower metallicities $-4.2 \leq$[Fe/H]< -3.0 and the RN91 sample ($N = 372$) for higher metallicities $-2.8 <$[Fe/H]$\leq +0.2$ under the assumption that the two samples are equally representative of the inner halo within the metallicity bin $-3.0 \leq$ [Fe/H]≤ -2.8. The error on the generic bin height has been estimated from the Poissonian error of its counterpart related to the parent sample. See text for further details.

[O/H] = 0.72 [Fe/H]		[O/H] = [Fe/H] + 0.70		ΔN		
ϕ	ψ	ϕ	ψ	fs10	H V	RN91
1.1322D−3	−1.4181D−1	4.0871D−4	+1.6168D−1	2	2	0
1.5774D−3		6.4776D−4		0	0	0
2.1976D−3		1.0266D−3		0	0	1
3.0615D−3	+2.0434D−1	1.6271D−3	+3.3983D−1	12	12	1
4.2652D−3	+6.3437D−1	2.5788D−3	+7.1386D−1	45	45	2
5.9421D−3	+7.0048D−1	4.0871D−3	+7.2397D−1	73	73	2
8.2783D−3	+8.9728D−1	6.4776D−3	+8.6477D−1	160	160	8
1.1533D−2	+9.6413D−1	1.0266D−2	+8.7562D−1	260	198	13
1.6067D−2	+1.0284D−0	1.6271D−2	+8.8390D−1	420	281	21
2.2384D−2	+9.4240D−1	2.5788D−2	+7.4189D−1	480	337	24
3.1185D−2	+9.4967D−1	4.0871D−2	+6.9316D−1	680	399	34
4.3445D−2	+9.1764D−1	6.4776D−2	+6.0513D−1	880	313	44
6.0526D−2	+9.2258D−1	1.0266D−1	+5.5407D−1	1240	231	62
8.4322D−2	+6.9376D−1	1.6271D−1	+2.6925D−1	1020	229	51
1.1747D−1	+4.7566D−1	2.5788D−1	−4.8510D−3	860	209	43
1.6366D−1	+1.4535D−1	4.0871D−1	−3.9116D−1	560	308	28
2.2800D−1	−3.3187D−1	6.4776D−1	−9.2438D−1	260	268	13
3.1764D−1	−5.1063D−1	1.0266D+0	−1.1591D−0	240	178	12
4.4253D−1	−8.8871D−1	1.6271D+0	−1.5932D−0	140	109	7
6.1651D−1	−1.1788D−0	2.5788D+0	−1.9393D−0	100	45	5
8.5890D−1		4.0871D+0		0	33	0
1.1966D−0	−2.1658D+0	6.4776D+0	−3.0383D−0	20	3	1
1.6670D−0		1.0266D+1		0	6	0

The main feature of the EDODs plotted in Fig. 4, is the presence of five regions characterized by a nearly linear trend, which will be named O, A, F, C, E, respectively, and defined in the following metallicity ranges, each containing $n_{\rm X}$ bins, X=O, A, F, C, E.

O [Fe/H] < -4.2; [Fe/H] > -0.2; $n_{\rm O} \rightarrow +\infty$; the distribution coincides with the horizontal axis after removing a single high-metallicity star from the RN91 sample, considered as due to disk contamination or, in any case, an outlier. On the other hand, the last appears in related tables and figures for comparison.

A $-4.2 \leq$ [Fe/H]≤ -2.7; $n_{\rm A} = 6$; the distribution is steep with positive slope.

F $-2.7 \leq$ [Fe/H] ≤ -1.7; $n_{\rm F} = 6$; the distribution is mild with negative slope.

C $-1.7 \leq$ [Fe/H]≤ -0.9; $n_{\rm C} = 5$; the distribution is steep with negative slope.

E $-0.9 \leq$ [Fe/H] ≤ -0.2; $n_{\rm E} = 4$; the distribution is less steep with negative slope.

In absence of LTE approximation with regard to the [O/H]-[Fe/H] empirical relation deduced from the Fal09 sample (case SH1), regions F and C may merge into a single region FC within the range $-2.7 \leq$ [Fe/H] ≤ -0.9 including $n_{\rm FC} = 10$ bins. The vertical bars on the horizontal axis mark [Fe/H] $= -2.2$, -1.6, and -0.8. The vertical dotted lines mark [Fe/H] $= -2.7$, -1.7, and -0.9, where the linear trend of the EDOD changes passing from a region to the adjacent one. Data points on the boundary between adjacent regions follow the linear trend exhibited by every of them.

The regression line related to the EDOD within each populated region, has been determined using the B model related to Table 2, under the assumption that the intrinsic scatter is dominant (Isobe et al. 1990). A single high-metallicity star from the RN91 sample, considered as due to disk contamination or, in any case, an outlier, has not been included in the fitting procedure. The regression line slope and intercept estimators and related

Table 4. Regression line slope and intercept estimators $\hat{a}$ and $\hat{b}$ and related dispersion estimators $\hat{\sigma}_{\hat{a}}$ and $\hat{\sigma}_{\hat{b}}$ for bisector regression models applied to the oxygen abundance distribution (EDOD) plotted in Fig. 4 with regard to different [O/H]-[Fe/H] empirical relations, deduced from the RB09 sample in presence of LTE approximation via Eq. (1) (top panel), and from the Fal09 sample in absence of LTE approximation, case SH1, via Eq. (2) (bottom panel). The method has been applied to each region (X) separately. Data points on the boundary between adjacent regions are used for determining regression lines within both of them.

X	$\hat{a}$	$\hat{\sigma}_{\hat{a}}$	$\hat{b}$	$\hat{\sigma}_{\hat{b}}$
A	+1.1382 E+2	2.0648 E+1	−1.0567 E−1	1.2296 E−1
F	−2.0950 E+0	7.2725 E−1	+1.0188 E+0	2.9109 E−2
C	−7.3565 E+0	1.2375 E−1	+1.3433 E+0	2.3577 E−2
E	−2.2569 E+0	1.0098 E−1	+1.7784 E−1	3.2148 E−2
A	+7.9432 E+1	1.9364 E+1	+2.7571 E−1	9.2608 E−2
F	−3.8855 E+0	6.1570 E−1	+8.9453 E−1	2.9691 E−2
C	−2.6460 E+0	1.4542 E−1	+7.3661 E−1	5.9411 E−2
FC	−2.8643 E+0	1.3796 E−1	+8.2804 E−1	2.7988 E−2
E	−5.3661 E−1	3.5681 E−2	−6.1514 E−1	4.3965 E−2

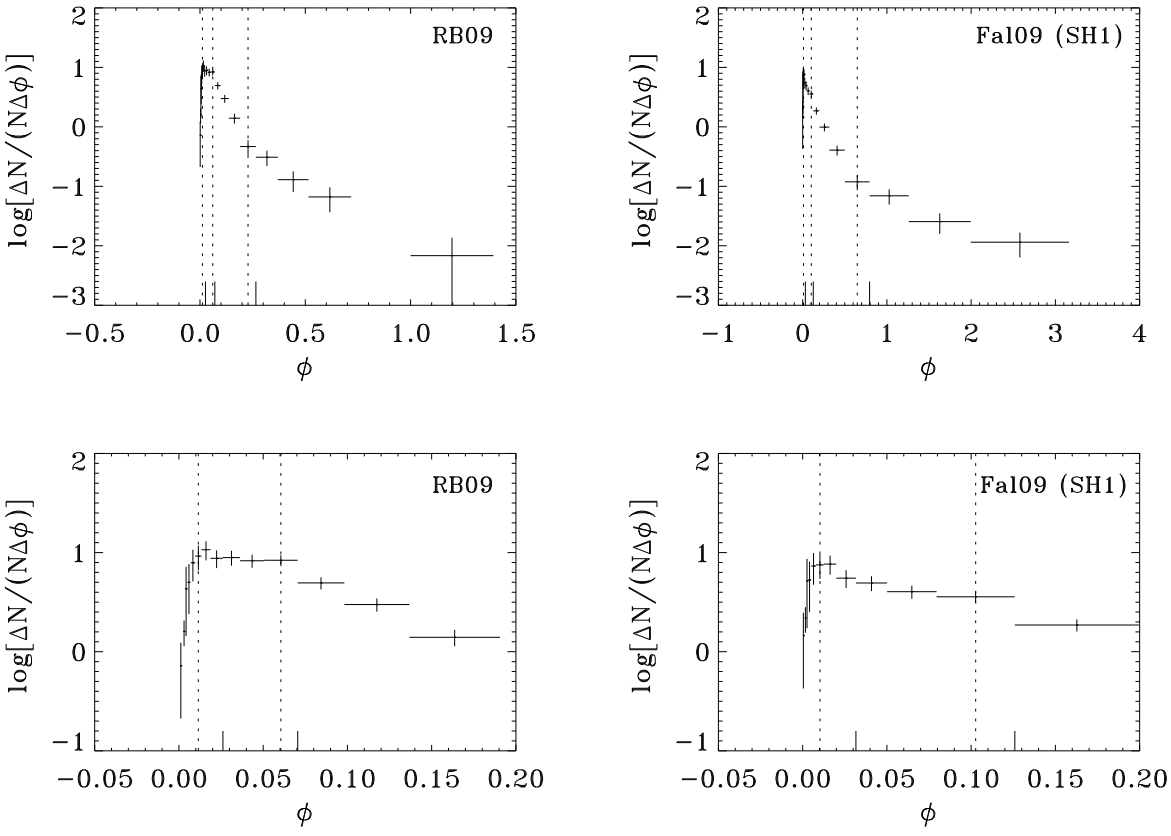

Fig. 4. *The empirical, differential oxygen abundance distribution (EDOD) related to the fs10 sample for [O/H]-[Fe/H] empirical relations deduced from the RB09 (left panels) and Fal09, case SH1 (right panels) sample. The whole distribution is represented in upper panels, while lower panels zoom the low-metallicity range. The uncertainty of the distribution is determined from Poisson errors. The vertical bars on the horizontal axis mark [Fe/H] = −2.2, −1.6, and −0.8. The vertical dotted lines mark [Fe/H] = −2.7, −1.7, and −0.9, where the linear trend of the EDOD changes passing from a region to the adjacent one. For further details refer to the text.*

Table 5. Transition points between adjacent regions, as determined from the intersection of related regression lines, for the oxygen abundance distribution (EDOD) plotted in Fig. 4 with regard to different [O/H]-[Fe/H] empirical relations, deduced from the RB09 sample in presence of LTE approximation via Eq. (1) (left panel) and from the Fal09 sample in absence of LTE approximation, case SH1, via Eq. (2) (right panel). In the latter case, the FC region has also been considered in alternative to F and C regions separately. For further details refer to the text.

	RB09		Fal09 (SH1)	
transition	ϕ	ψ	ϕ	ψ
O-A	9.4624 E−4	+2.0383 E−3	3.1623 E−4	+3.0083 E−1
A-F	9.7001 E−3	+9.9844 E−1	7.4271 E−3	+8.6567 E−1
F-C	6.1687 E−2	+8.8953 E−1	1.2740 E−1	+9.9952 E−1
C-E	2.2854 E−1	−3.3795 E−1	6.4083 E−1	−9.5902 E−1
E-O	7.1779 E−1	−1.4421 E−0	3.1623 E−0	−2.3121 E−0
A-FC			6.7114 E−3	+8.0882 E−1
FC-E			6.2002 E−1	−9.4785 E−1

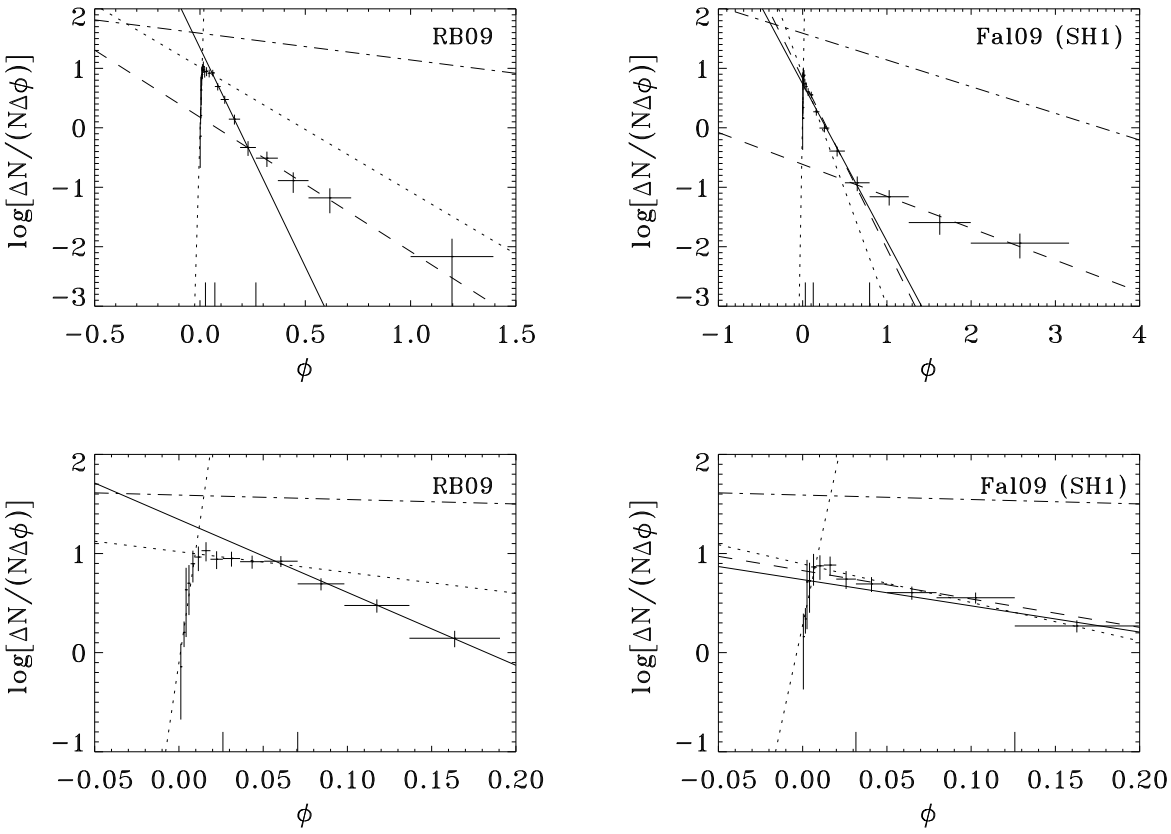

Fig. 5. *Regression lines to the empirical differential oxygen abundance distribution (EDOD) plotted in Fig. 4, with regard to the regions (from the left to the right): A (dotted, positive slope, $n_A = 6$), F(dotted, negative slope, $n_F = 6$), C (full, $n_C = 5$), E (dashed, $n_E = 4$). The more inclined dashed line in right panels corresponds to the FC ($n_{FC} = 10$) region, in alternative to F and C regions separately. Other captions as in Fig. 4. For further details refer to the text.*

dispersion estimators are listed in Table 4 for each region of the EDODs plotted in Fig. 4. The results are consistent (within $\mp\sigma$) with their counterparts determined using the other models mentioned above.

The selection of a special method is of little relevance, due to the paucity of data within each region.

The regression lines are represented in Fig. 5 for each region (from the left to the right): A (dotted, positive slope), F(dotted, negative slope), C (full), E (dashed), with regard to the EDOD plotted in Fig. 4.

In absence of LTE approximation, the case SH1 (right panels), a more inclined dashed line fits to the FC region, in alternative to F and C regions separately. To ensure continuity, the above mentioned regions must be redefined by the intersections of regression lines which make the transition from a selected region to the adjacent one. The results are listed in Table 5 for the EDOD and related regression lines are plotted in Fig. 5.

A vertical line instead of a regression line has been considered for the O region, where no data exist.

In conclusion, the EDOD related to the inner halo may be approximated to a satisfactory extent as due to the contribution of four (A, F, C, E) or three (A, FC, E) regions within which the trend is linear. An interpretations in terms of simple models of chemical evolution is highly attractive, as the corresponding TDOD shows, in fact, a linear trend (Pagel 1989, Rocha-Pinto and Maciel 1996, C00, C01, C07).

3. THE MODEL

In their original formulation, simple models of chemical evolution are closed-box (CB) i.e. mass conservation (gas + stars) holds (e.g. Searle and Sargent 1972, Pagel and Patchett 1975). In later formulation, a "reservoir" is added to the "box" where mass conservation no longer occurs within the box but still holds within the system box + reservoir. Accordingly, related models can be conceived as closed-(box+reservoir) (CBR) models. The "reservoir" defined in the current attempt is different from its counterpart conceived in models of cosmological cold gas accretion (e.g. Bouché et al. 2010).

The gas within the box is "active" in the sense that allows for star formation according to a specified birth-rate stellar function. The gas within the reservoir is "inhibited" in the sense that no star formation takes place. Gas may outflow from the box into the reservoir (H76) or inflow into the box from the reservoir (C07). The related TDOD is a straight line under the restriction that the flowing gas has equal oxygen abundance with respect to the pre existing gas. The related slope (to the knowledge of the author) is negative in all cases studied in literature (e.g. Pagel 1989, Rocha-Pinto and Maciel 1996, C00, C01, C07).

For this reason, the formulation of CBR models shall be extended to a TDOD with positive slope, under the standard assumptions of CB models: (i) instantaneous recycling within the box, where stars are divided into two categories, namely: (a) short-lived, which instantaneously evolve, and (b) long-lived, all of which are still evolving; (ii) instantaneous mixing within the box, where the gas returned from short-lived stars is instantaneously mixed with the interstellar medium yielding uniform composition; and the standard assumptions of CBR models; (iii) mass conservation within the system (box+reservoir); (iv) gas outflow from the box into the reservoir or inflow into the box from the reservoir, at a rate proportional to the star formation rate; (v) inhibition of star formation within the reservoir; (vi) gas outflow or inflow with fixed composition (in particular, equal) with respect to the pre existing gas.

In this picture, the oxygen (or any other primary element) mass fraction can be determined, extending the procedure followed for CB models (e.g. Pagel and Patchett 1975, Wang and Silk 1993, C00) to CBR models.

3.1. Basic theory

The change in oxygen (or any other primary element) gas mass $M_{\rm gO}$ is owing to four contributions:

$$\frac{{\rm d}M_{\rm gO}}{{\rm d}t} = \left(\frac{{\rm d}M_{\rm gO}}{{\rm d}t}\right)_{\rm sf} + \left(\frac{{\rm d}M_{\rm gO}}{{\rm d}t}\right)_{\rm gr} + \left(\frac{{\rm d}M_{\rm gO}}{{\rm d}t}\right)_{\rm sdu} + \left(\frac{{\rm d}M_{\rm gO}}{{\rm d}t}\right)_{\rm sds} \quad , (10)$$

related to subtraction via star formation (sf), subtraction via outflow from the box into the reservoir or addition via inflow into the box from the reservoir (gr), addition via unsynthesised gas from short-lived stars (sdu), and addition via newly synthesised gas from short-lived stars (sds), respectively. In this picture, at any step, dying (e.g. AGB) stars return part of their material to the interstellar medium which, at the next step, may undergo outflow.

For simple CBR models, the following relations hold:

$$\frac{{\rm d}M_{\rm g}}{{\rm d}t} = -\alpha\frac{{\rm d}M_{\rm S}}{{\rm d}t} - \kappa\alpha\frac{{\rm d}M_{\rm S}}{{\rm d}t} = -\alpha(1+\kappa)\frac{{\rm d}M_{\rm S}}{{\rm d}t} \quad (11)$$

$$\left(\frac{{\rm d}M_{\rm gO}}{{\rm d}t}\right)_{\rm sf} + \left(\frac{{\rm d}M_{\rm gO}}{{\rm d}t}\right)_{\rm gr} + \left(\frac{{\rm d}M_{\rm gO}}{{\rm d}t}\right)_{\rm sdu} =$$

$$= -Z_{\rm O}\alpha(1+\zeta_{\rm O}\kappa)\frac{{\rm d}M_{\rm S}}{{\rm d}t} \quad , \quad (12)$$

$$\left(\frac{{\rm d}M_{\rm gO}}{{\rm d}t}\right)_{\rm sds} = (1-Z)\hat{p}\alpha\frac{{\rm d}M_{\rm S}}{{\rm d}t} \quad , \quad (13)$$

where $M_{\rm g}$ is the mass in active gas, $M_{\rm S}$ is the global mass in gas which has been turned into stars, $M_{\rm gO}$ is the oxygen mass in active gas, α is the fraction in long-lived stars and stellar remnants within a star generation (lock parameter), $\zeta_{\rm O}$ is the oxygen abundance ratio of flowing to pre existing gas (cut parameter), κ is the ratio of flowing (outflow from the

box into the reservoir or inflow into the box from the reservoir) gas rate to locking (in the form of long-lived stars and stellar remnants) gas rate (flow parameter), $Z_{\rm O}$ and Z are the oxygen and metal mass abundance, respectively, within the active gas, and $\hat{p}$ is the ratio of the oxygen mass newly synthesised and returned to the interstellar medium for a metal-free initial composition[2], to the mass locked up in long-lived stars and stellar remnants (yield parameter). The lock parameter α, the cut parameter $\zeta_{\rm O}$, the flow parameter κ, and the yield parameter $\hat{p}$, for the sake of brevity, in the following will be quoted as lock, cut, flow, and yield, respectively.

The definition of the oxygen mass abundance $Z_{\rm O}$, fractional active gas mass μ, and fractional star mass s, read:

$$Z_{\rm O} = \frac{M_{\rm gO}}{M_{\rm g}} \quad , \quad \mu = \frac{M_{\rm g}}{M_0} \quad , \quad s = \alpha S = \frac{\alpha M_{\rm S}}{M_0} = \frac{M_{\rm s}}{M_0} \quad , \tag{14}$$

where $M_{\rm s} = \alpha M_{\rm S}$ is the mass in long-lived stars and stellar remnants, and M_0 is the total mass within the box at the starting configuration.

The substitution of Eqs. (11)-(13) into (10) yields:

$$\frac{{\rm d}M_{\rm gO}}{{\rm d}t} = \left[\frac{1+\zeta_{\rm O}\kappa}{1+\kappa} Z_{\rm O} - \frac{1-Z}{1+\kappa}\hat{p}\right] \frac{{\rm d}M_{\rm g}}{{\rm d}t} = \\ = \left[Z_{\rm O} + \frac{(\zeta_{\rm O}-1)\kappa}{1+\kappa} Z_{\rm O} - \frac{1-Z}{1+\kappa}\hat{p}\right] \frac{{\rm d}M_{\rm g}}{{\rm d}t} \quad , \tag{15}$$

and the fractional oxygen gas mass, via Eq. (14) reads:

$$\frac{M_{\rm gO}}{M_0} = \frac{M_{\rm gO}}{M_{\rm g}} \frac{M_{\rm g}}{M_0} = Z_{\rm O}\mu \quad , \tag{16}$$

where, in addition:

$$\frac{{\rm d}(Z_{\rm O}\mu)}{{\rm d}t} = Z_{\rm O}\frac{{\rm d}\mu}{{\rm d}t} + \mu\frac{{\rm d}Z_{\rm O}}{{\rm d}t} \quad , \tag{17}$$

on the other hand, in terms of fractional masses, Eq. (15) may be cast into the equivalent form:

$$\frac{{\rm d}(Z_{\rm O}\mu)}{{\rm d}t} = \left[Z_{\rm O} + \frac{(\zeta_{\rm O}-1)\kappa}{1+\kappa} Z_{\rm O} - \frac{1-Z}{1+\kappa}\hat{p}\right] \frac{{\rm d}\mu}{{\rm d}t} \quad , \tag{18}$$

and the combination of Eqs. (17) and (18) yields:

$$\frac{{\rm d}Z_{\rm O}}{(1-Z) + (1-\zeta_{\rm O})(\kappa/\hat{p})Z_{\rm O}} = -\hat{p}''\frac{{\rm d}\mu}{\mu} \quad , \tag{19}$$

$$\hat{p}'' = \frac{\hat{p}}{1+\kappa} \quad , \tag{20}$$

where $\hat{p}''$ is the effective yield parameter, hereafter quoted as the effective yield (H76).

A linear dependence of metal abundance on oxygen abundance:

$$Z = A_{\rm O} Z_{\rm O} \quad , \tag{21}$$

allows analytical integration and, in addition, implies oxygen nucleosynthesis within the first generation of stars, in agreement with current theories predicting massive Pop III stars. For the protosolar nebula, $Z_{\rm O} \approx 2.7 Z_{\rm C}$ and $Z - Z_{\rm O} - Z_{\rm C} \approx 2 Z_{\rm C}$ from recent investigations (Asplund et al. 2009) where $Z_{\rm C}$ is the carbon abundance. Accordingly, $A_{\rm O} = Z/Z_{\rm O} \approx 2$ and $A_{\rm O} = 2$ will be used in the following. An opposite choice, $A_{\rm O} = 0$, is equivalent to $Z << 1$ i.e. neglecting the metal abundance with respect to unity, as usually done in dealing with simple models.

The combination of Eqs. (19) and (21) produces:

$$\frac{{\rm d}(c\phi)}{1-c\phi} = -c\frac{\hat{p}''}{(Z_{\rm O})_\odot}\frac{{\rm d}\mu}{\mu} \quad , \tag{22}$$

$$\phi = \frac{Z_{\rm O}}{(Z_{\rm O})_\odot} \quad , \quad c = \frac{(Z_{\rm O})_\odot}{\hat{p}}\left[A_{\rm O}\hat{p} - \kappa(1-\zeta_{\rm O})\right] , \tag{23}$$

and the solution of Eq. (22), after some algebra, is:

$$c\phi - c\phi_i = [1 - c\phi_i]\left[1 - \left(\frac{\mu}{\mu_i}\right)^{c\hat{p}''/(Z_{\rm O})_\odot}\right] \quad , \tag{24}$$

where the index i denotes the starting configuration at the cosmic time, t_i. Reversing the role of the variables, Eq. (24) reads:

$$\frac{\mu}{\mu_i} = \left[\frac{1-c\phi}{1-c\phi_i}\right]^{(Z_{\rm O})_\odot/(c\hat{p}'')} \quad , \tag{25}$$

which is monotonic in $c\phi$.

Using the MacLaurin series expansion:

$$\left(\frac{\mu}{\mu_i}\right)^{c\hat{p}''/(Z_{\rm O})_\odot} = \exp\left[\frac{c\hat{p}''}{(Z_{\rm O})_\odot}\ln\frac{\mu}{\mu_i}\right] = \\ = 1 + \frac{c\hat{p}''}{(Z_{\rm O})_\odot}\ln\frac{\mu}{\mu_i} + ... \quad , \tag{26}$$

under the further assumption that the terms of higher order with respect to the second can be neglected, Eq. (24) reduces to:

$$\phi - \phi_i = -(1-c\phi_i)\frac{\hat{p}''}{(Z_{\rm O})_\odot}\ln\frac{\mu}{\mu_i} \quad , \tag{27}$$

$$\left|\frac{c\hat{p}''}{(Z_{\rm O})_\odot}\ln\frac{\mu}{\mu_i}\right| \le \left|\frac{c\hat{p}''}{(Z_{\rm O})_\odot}\ln\frac{\mu_f}{\mu_i}\right| << 1 \quad , \tag{28}$$

where the index f, denotes the ending configuration at the cosmic time t_f, and $\mu_i < \mu < \mu_f$ or $\mu_i > \mu > \mu_f$ owing to Eq. (25) provided $\kappa \neq -1$. The special cases $\kappa = -1$ and $|\kappa| >> 1$, $\kappa_{\rm O} = 0$, are analysed in Appendix A1 and A2, respectively.

[2]This detail is usually omitted in literature.

If the product $c\phi_i$ is negligible with respect to unity, Eq. (27) reduces to:

$$\phi - \phi_i = -\frac{\hat{p}''}{(Z_{\rm O})_\odot} \ln \frac{\mu}{\mu_i} \quad , \tag{29}$$

$$|c\phi_i| = \left| \frac{(Z_{\rm O})_\odot}{\hat{p}} \phi_i [A_{\rm O}\hat{p} - \kappa(1-\zeta_{\rm O})] \right| =$$

$$= \left| \frac{\phi_i}{\phi_{\rm max} - \phi_i} \left[A_{\rm O}\hat{p}'' - \frac{\kappa(1-\zeta_{\rm O})}{1+\kappa} \right] \right| << 1 \quad , \tag{30}$$

where $\phi_{\rm max} = \phi_i + \hat{p}''/(Z_{\rm O})_\odot$ corresponds to the maximum of the cumulative oxygen abundance distribution (e.g. Prantzos, 2010). The classical formulation (H76) is formally coincident with Eq. (29) in the special case of outflowing gas ($\kappa > 0$) with equal composition with respect to the pre existing gas ($\zeta_{\rm O} = 1$).

Oxygen abundances expressed by Eq. (27) or (29) make a viable approximation with respect to the general case Eq. (24) for values of the cut very close to unity $|\zeta_{\rm O} - 1| << 1$. If otherwise, the related inequalities Eqs. (28) and (30) must be verified.

It is worth emphasyzing that the inequality Eq. (28) does not affect the instantaneous recycling approximation but only the general formulation expressed by Eq. (24) provided the $Z_{\rm O}$-Z relation is linear, according to Eq. (21). In general, it is assumed the instantaneou recycling approximation holds for sufficiently high fractional active gas mass fraction, $\mu \gtrsim 0.1$ (e.g. Prantzos 2007, Fig. 12 therein) but the threshold could be lowered using Eq. (24) instead of Eq. (27). In fact, neglecting the terms of higher order in the MacLaurin series Eq. (26), makes the oxygen abundance $Z_{\rm O}$, increased with respect to the general case Eq. (24).

In terms of fractional masses, Eq. (11) via Eq. (14) may be cast into the equivalent form:

$$\alpha(1+\kappa)\frac{{\rm d}S}{{\rm d}t} = (1+\kappa)\frac{{\rm d}s}{{\rm d}t} = -\frac{{\rm d}\mu}{{\rm d}t} \quad , \tag{31}$$

which can be read in the following way: any mass change in active gas is counterbalanced by a change in long-lived stars and stellar remnants plus a change in gas outflow from the box into the reservoir ($\kappa > 0$) or a change in gas inflow into the box from the reservoir ($\kappa < 0$). More specifically, a number of different flow regimes may be distinguished as listed below.

- Outflow regime ($\kappa > 0$) where star formation is inhibited (H76). For an exhaustive description refer to earlier attempts (C00, C01).
- Stagnation regime ($\kappa = 0$) where star formation is neither inhibited nor enhanced. Accordingly, CBR models reduce to CB models. For an exhaustive description refer to earlier attempts (Searle and Sargent 1972, Pagel and Patchett 1975).
- Moderate inflow regime ($-1 < \kappa < 0$) where star formation is enhanced and active gas mass fraction monotonically decreases in time. For an exhaustive description refer to an earlier attempt (C07).
- Steady inflow regime ($\kappa = -1$) where star formation is enhanced and active gas mass fraction remains unchanged.
- Strong inflow regime ($\kappa < -1$) where star formation is enhanced and active gas mass fraction monotonically increases in time.

The effective yield $\hat{p}''$, defined by Eq. (20), cannot exceed the real yield $\hat{p}$, both in the outflow and in strong inflow regime while the contrary holds in a moderate inflow regime and, *a fortiori*, in the steady inflow regime where a divergency occurs. For this reason, the effective yield cannot be considered alone but together with the factor $\ln[\mu/(\mu)_i]$. More specifically, the right-hand side of Eq. (29), $-\hat{p}'' \ln[\mu/(\mu)_i] = -\hat{p} \ln[\mu/(\mu)_i]/(1+\kappa)$, is positive in all regimes due to the trend exhibited by the active gas mass fraction. In the steady inflow regime, the following relation necessarily holds:

$$\lim_{\kappa \to -1} \left[\frac{\ln(\mu/\mu_i)}{\ln(\mu_f/\mu_i)} \right] = \frac{\phi - \phi_i}{\phi_f - \phi_i} = \frac{t - t_i}{t_f - t_i} \quad , \tag{32}$$

in terms of the normalized oxygen abundance related to a constant active gas mass fraction, or in terms of the cosmic time. For a formal demonstration refer to Appendix A1.

In any case, the mass conservation follows from integration of Eq. (31) as:

$$\mu + s + D = \mu_0 + s_0 + D_0 = \mu_0 = 1 \quad , \tag{33}$$

$$D = \alpha\kappa S = \kappa s \quad , \tag{34}$$

conformly to Eq. (14) where D is the gas mass fraction which outflowed from the box into the reservoir ($\kappa > 0$) or inflowed into the box from the reservoir ($\kappa < 0$). An equivalent form of Eq. (33) reads:

$$\mu + s = 1 - D \quad , \tag{35}$$

where variables on the left and the right-hand side member relate to the box and the reservoir, respectively.

The birth-rate stellar function (number of stars born per unit volume, mass, and time), needs to be specified for determining the temporal behaviour of gas and star fractional masses. Following an earlier attempt (C00), the selected choice reads:

$$\mathcal{B}(\widetilde{m}, \widetilde{t}) = \frac{B}{V} f(\mu) \Phi(\widetilde{m}) \ , \quad \widetilde{m} = \frac{m}{m_\odot} \ , \quad \widetilde{t} = \frac{t}{\rm Gyr} \ , \tag{36}$$

where B is a normalization constant, V the volume of the box, $\Phi(\widetilde{m})$ the stellar initial mass function and $f(\mu)$ an assigned function of the active gas mass fraction which is a time-dependent term. The number of stars born per unit volume within an infinitesimal dimensionless mass range $\widetilde{m} \mp {\rm d}\widetilde{m}/2$ and infinitesimal dimensionless time range $\widetilde{t} \mp {\rm d}\widetilde{t}/2$ is $\mathcal{B}(\widetilde{m}, \widetilde{t})\, {\rm d}\widetilde{m}\, {\rm d}\widetilde{t}$.

The number of long-lived stars generated (within the box) up to an assigned dimensionless cosmic time $\widetilde{t}$ is:

$$N_{\ell\ell}(\widetilde{t}) = \int_{\widetilde{t}_i}^{\widetilde{t}} \mathrm{d}\widetilde{t} \int_{\widetilde{m}_{\mathrm{mf}}}^{\widetilde{m}_{\ell\ell}} V\mathcal{B}(\widetilde{m},\widetilde{t})\,\mathrm{d}\widetilde{m} = \\ = BF(\widetilde{t})I'(5) \quad , \tag{37a}$$

$$F(\widetilde{t}) = \int_{\widetilde{t}_i}^{\widetilde{t}} f(\mu)\,\mathrm{d}\widetilde{t}; \quad I'(5) = \int_{\widetilde{m}_{\mathrm{mf}}}^{\widetilde{m}_{\ell\ell}} \Phi(\widetilde{m})\,\mathrm{d}\widetilde{m}, \tag{37b}$$

where m_{mf} is the lower stellar mass limit, and $m_{\ell\ell}$ the upper mass limit of long-lived stars related to the assumption of instantaneous recycling.

The mass fraction in stars globally generated (within the box) up to a dimensionless cosmic time $\widetilde{t}$ is:

$$S(\widetilde{t}) = \int_{\widetilde{t}_i}^{\widetilde{t}} \mathrm{d}\widetilde{t} \int_{\widetilde{m}_{\mathrm{mf}}}^{\widetilde{m}_{\mathrm{Mf}}} \frac{Vm_\odot}{M_0}\widetilde{m}\mathcal{B}(\widetilde{m},\widetilde{t})\,\mathrm{d}\widetilde{m} = \\ = CF(\widetilde{t}) \quad , \tag{38a}$$

$$C = \frac{Bm_\odot}{M_0} I(1) \; ; \quad I(1) = \int_{\widetilde{m}_{\mathrm{mf}}}^{\widetilde{m}_{\mathrm{Mf}}} \widetilde{m}\Phi(\widetilde{m})\,\mathrm{d}\widetilde{m} \; , \tag{38b}$$

where m_{Mf} is the upper stellar mass limit.

The mass fraction in long-lived stars and in gas outflowed from the box into the reservoir or inflowed into the box from the reservoir, at an assigned dimensionless cosmic time $\widetilde{t}$ are:

$$s(\widetilde{t}) = \alpha S(\widetilde{t}) = \alpha C F(\widetilde{t}) \quad , \tag{39}$$

$$D(\widetilde{t}) = \alpha\kappa S(\widetilde{t}) = \alpha\kappa C F(\widetilde{t}) \quad , \tag{40}$$

according to the definition of lock and flow, respectively.

The star formation rate (within the box), lock rate, and flow rate at an assigned dimensionless cosmic time $\widetilde{t}$ are:

$$\frac{\mathrm{d}S}{\mathrm{d}\widetilde{t}} = Cf(\mu) \quad , \tag{41}$$

$$\frac{\mathrm{d}s}{\mathrm{d}\widetilde{t}} = \alpha C f(\mu) \quad , \tag{42}$$

$$\frac{\mathrm{d}D}{\mathrm{d}\widetilde{t}} = \alpha\kappa C f(\mu) \quad , \tag{43}$$

and the combination of Eqs. (31) and (41) yields:

$$\alpha(1+\kappa)Cf(\mu) = -\frac{\mathrm{d}\mu}{\mathrm{d}\widetilde{t}} \quad , \tag{44}$$

which is equivalent to:

$$\int_{\mu_i}^{\mu} \frac{\mathrm{d}\mu}{f(\mu)} = -\alpha(1+\kappa)C(\widetilde{t}-\widetilde{t}_i) \quad , \tag{45}$$

in the special case $f(\mu) = \mu$, Eq. (45) can be integrated as:

$$\mu = \mu_i \exp[-\alpha(1+\kappa)C(\widetilde{t}-\widetilde{t}_i)] \quad , \tag{46}$$

and the combination of Eqs. (20), (29), and (46) yields a linear trend for the oxygen abundance:

$$\phi - \phi_i = \frac{\hat{p}\alpha C}{(Z_{\mathrm{O}})_\odot}(\widetilde{t}-\widetilde{t}_i) \quad , \tag{47}$$

regardless of the flow κ.

In the more general case $f(\mu) = \mu^\nu$, Eq. (41) reduces to a Schmidt (1959, 1963) star formation law. Leaving aside the above discussed special case $\nu = 1$, Eq. (45) can be integrated and, after some algebra, the result is:

$$\mu = \mu_i \left[1 - \frac{1-\nu}{\mu_i^{1-\nu}}\alpha(1+\kappa)C(\widetilde{t}-\widetilde{t}_i)\right]^{1/(1-\nu)} \quad , \; \nu \neq 1; \tag{48}$$

which, using the logarithm MacLaurin series $\ln(1+x) = x - x^2/2 + x^3/3 - ...$, $\mid x \mid < 1$, and neglecting the terms of higher order with respect to the first, may be approximated as:

$$\mu = \mu_i \exp\left[-\mu_i^{\nu-1}\alpha(1+\kappa)C(\widetilde{t}-\widetilde{t}_i)\right] \quad , \tag{49a}$$

$$\left|(1-\nu)\mu_i^{\nu-1}\alpha(1+\kappa)C(\widetilde{t}-\widetilde{t}_i)\right| << 1 \quad , \tag{49b}$$

in the limit, $\nu \to 1$, Eqs. (46) and (49a) coincide as expected. The combination of Eqs. (20), (29), and (49) yields:

$$\phi - \phi_i = \frac{\hat{p}\alpha\mu_i^{\nu-1}C}{(Z_{\mathrm{O}})_\odot}(\widetilde{t}-\widetilde{t}_i) \quad , \tag{50}$$

regardless of the flow κ. Then, a Schmidt star formation law with exponent $\nu \approx 1$ implies a linear dependence of the oxygen (or any other primary element) abundance on the cosmic time.

In general, simple CBR models are described by Eqs. (29) and (45), the latter only for including the temporal behaviour. It is worth noticing the star formation history of galaxies (as indicated by hydrodynamical simulations) is insensitive to the assumed star formation law (e.g. Katz et al. 1996, Schaye et al. 2010, Davé et al. 2011).

3.2. Theoretical differential oxygen abundance distribution (TDOD)

For a selected spectral class, the number of long-lived stars generated (within the box) up to an assigned dimensionless cosmic time, is:

$$N(\widetilde{t}) = \int_{\widetilde{t}_i}^{\widetilde{t}} \mathrm{d}\widetilde{t} \int_{\widetilde{m}_1}^{\widetilde{m}_2} V\mathcal{B}(\widetilde{m},\widetilde{t}) = C_{12}F(\widetilde{t}) \quad , \tag{51a}$$

$$C_{12} = BI'(1,2) \; ; \quad I'(1,2) = \int_{\widetilde{m}_1}^{\widetilde{m}_2} \Phi(\widetilde{m})\,\mathrm{d}\widetilde{m} \; , \tag{51b}$$

where m_1 and m_2 are the lower and upper mass limit of the spectral class.

For simple CBR models, the oxygen abundance is monotonically increasing in time owing to the assumption of instantaneous recycling, which implies the number of stars born up to the cosmic time t coincides with the number of stars with normalized oxygen abundance up to the related value $\phi(t)$, or $N(t) = N(\phi)$. The same holds for the long-lived star mass fraction (including stellar remnants) $s(t) = s(\phi)$. By use of Eq. (14), the long-lived star mass fraction and the number of long-lived stars $N_{\ell\ell}$ can be related as:

$$\frac{s - s_i}{s_f - s_i} = \frac{\overline{m}N_{\ell\ell} - \overline{m}(N_{\ell\ell})_i}{\overline{m}(N_{\ell\ell})_f - \overline{m}(N_{\ell\ell})_i} \quad , \tag{52}$$

where $\overline{m} = M_s/N_{\ell\ell}$ is the mean mass of long-lived stars (including stellar remnants). Under the assumption of a universal stellar initial mass function, the fraction of long-lived stars belonging to a selected spectral class with respect to the total, maintains unchanged $N_{\ell\ell}/N = \text{const}$ and Eq. (52) translates into (Pagel and Patchett 1975):

$$\frac{s - s_i}{s_f - s_i} = \frac{N - N_i}{N_f - N_i} \quad , \tag{53}$$

in addition, the combination of Eqs. (33) and (34) yields:

$$(1 + \kappa)s = 1 - \mu \quad , \tag{54}$$

accordingly, Eq. (53) may be cast into the equivalent form:

$$\frac{N - N_i}{N_f - N_i} = \frac{1 - \mu/\mu_i}{1 - \mu_f/\mu_i} \quad , \tag{55}$$

where the ratio μ/μ_i is expressed by Eq. (29) with respect to the normalized oxygen abundance ϕ and by Eqs. (46) and (48) with respect to the dimensionless cosmic time $\widetilde{t}$ in the last case restricting to a Schmidt star formation law.

The derivation of Eqs. (53) and (55) with respect to ϕ yields:

$$\begin{aligned} \frac{\mathrm{d}N}{(N_f - N_i)\,\mathrm{d}\phi} &= \frac{\mathrm{d}s}{(s_f - s_i)\,\mathrm{d}\phi} \\ &= \frac{-\,\mathrm{d}(\mu/\mu_i)}{(1 - \mu_f/\mu_i)\,\mathrm{d}\phi}, \end{aligned} \tag{56}$$

which, using Eq. (25), takes the explicit form:

$$\begin{aligned} \frac{\mathrm{d}N}{(N_f - N_i)\,\mathrm{d}\phi} = \frac{\mu_i}{\mu_i - \mu_f}\frac{(Z_\mathrm{O})_\odot}{\hat{p}''}\frac{1}{1 - c\phi_i} \times \\ \times \left[\frac{1 - c\phi}{1 - c\phi_i}\right]^{(Z_\mathrm{O})_\odot/(c\hat{p}'') - 1} \quad , \end{aligned} \tag{57}$$

where the decimal logarithm of the left-hand side is defined as the TDOD (Pagel 1989, C00, C01):

$$\begin{aligned} \psi(\phi) &= \log \frac{\mathrm{d}N}{(N_f - N_i)\,\mathrm{d}\phi} = \\ &= \left[\frac{(Z_\mathrm{O})_\odot}{c\hat{p}''} - 1\right]\log(1 - c\phi) + b \quad , \end{aligned} \tag{58}$$

$$b = \log\left[\frac{\mu_i}{\mu_i - \mu_f}\frac{(Z_\mathrm{O})_\odot}{\hat{p}''}\right] - \frac{(Z_\mathrm{O})_\odot}{c\hat{p}''}\log(1 - c\phi_i), \tag{59}$$

which is represented as a curve on the $(\mathsf{O}\phi\psi)$ plane. The related intercept is $\psi(0) = b$.

In the linear approximation $c \to 0$ the series development:

$$\log(1 - c\phi) = \frac{1}{\ln 10}\left[-c\phi + \frac{(c\phi)^2}{2} - \frac{(c\phi)^3}{3} + ...\right], \tag{60}$$

can be truncated to the first term and Eqs. (58) and (59) reduce to:

$$\psi(\phi) = a\phi + b \quad , \tag{61}$$

$$a = -\frac{1}{\ln 10}\frac{(Z_\mathrm{O})_\odot}{\hat{p}''} \quad , \tag{62}$$

$$b = \log\left[\frac{\mu_i}{\mu_i - \mu_f}(-\ln 10)a\right] - a\phi_i \quad , \tag{63}$$

which is represented as a straight line on the $(\mathsf{O}\phi\psi)$ plane. The TDOD slope a, defined by Eq. (62), depends on the flow regime discussed above. More specifically, $a < 0$ in both the outflow regime and moderate inflow regime; $a = 0$ in the steady inflow regime; $a > 0$ in the strong inflow regime. The TDOD intercept b, defined by Eq. (63), must necessarily fulfill the condition $\mu_f > 0$ which implies the inequality:

$$b > b(\mu_f = 0) = \log(-\ln 10\, a) - a\phi_i \,;\; a < 0 \,, \tag{64}$$

on the other hand, $\mu_f > 0$ directly follows from $a \geq 0$. The above considerations can be extended to the nonlinear case.

3.3. Fitting to empirical differential oxygen abundance distribution (EDOD)

Both the EDOD and the TDOD can be represented in the $(\mathsf{O}\phi\psi)$ plane, but the related normalizations are different. More specifically, the former is normalized to the sample population N, according to Eq. (8), while the latter is normalized to the computed long-lived star population $N_f - N_i$, according to Eq. (58). Then, the EDOD and the TDOD differ by a normalization constant $\log C_N$, which must be taken into consideration in performing the fitting procedure. In other words, the TDOD ψ_T, has to be vertically shifted in the $(\mathsf{O}\phi\psi)$ plane by a value $\log C_N$ for matching to the EDOD ψ_E. The shifted TDOD intercept, via Eqs. (59) and (63), translates into:

$$\begin{aligned} b_\mathrm{N} = b + \log C_\mathrm{N} = \log\left[\frac{C_\mathrm{N}\mu_i}{\mu_i - \mu_f}\frac{(Z_\mathrm{O})_\odot}{\hat{p}''}\right] - \\ - \frac{(Z_\mathrm{O})_\odot}{c\hat{p}''}\log(1 - c\phi_i) \quad , \end{aligned} \tag{65}$$

in the general case, and:

$$b_{\rm N} = b + \log C_{\rm N} = \\ = \log\left[\frac{C_{\rm N}\mu_i}{\mu_i - \mu_f}\frac{(Z_{\rm O})_\odot}{\hat{p}''}\right] + \frac{1}{\ln 10}\frac{(Z_{\rm O})_\odot}{c\hat{p}''}\phi_i \quad , \quad (66)$$

in the linear case. The EDOD intercept $b_{\rm N}$ can be deduced from the fit to the data.

The particularization of Eq. (25) and (29) to the final configuration reads:

$$\frac{\mu_f}{\mu_i} = \left[\frac{1-c\phi_f}{1-c\phi_i}\right]^{(Z_{\rm O})_\odot/(c\hat{p}'')} \quad , \quad (67)$$

in the general case, and:

$$\frac{\mu_f}{\mu_i} = \exp\left[-\frac{(Z_{\rm O})_\odot}{\hat{p}''}(\phi_f - \phi_i)\right] \quad , \quad (68)$$

in the linear case.

The combination of Eqs. (65) and (67) yields:

$$C_{\rm N} = 10^{b_{\rm N}}\frac{\hat{p}''}{(Z_{\rm O})_\odot}\left[1 - \left(\frac{1-c\phi_f}{1-c\phi_i}\right)^{(Z_{\rm O})_\odot/(c\hat{p}'')}\right] \times \\ \times (1-c\phi_i)^{(Z_{\rm O})_\odot/(c\hat{p}'')} \quad , \quad (69)$$

in the linear case $c \to 0$ using a fundamental limit yields:

$$\lim_{c\to 0}(1-c\phi)^{(Z_{\rm O})_\odot/(c\hat{p}'')} = \exp\left[-\frac{(Z_{\rm O})_\odot}{\hat{p}''}\phi\right] = \\ = \exp_{10}\left[-\frac{1}{\ln 10}\frac{(Z_{\rm O})_\odot}{\hat{p}''}\phi\right] . \quad (70)$$

Accordingly, Eq. (69) after some algebra reduces to:

$$C_{\rm N} = -\frac{1}{\ln 10}\frac{1}{a}\exp_{10}(a\phi_i + b_{\rm N})\{1 - \exp_{10}[a(\phi_f - \phi_i)]\} \quad , \quad (71)$$

where a is defined by Eq. (62) and $b_{\rm N}$ can be determined from the knowledge of the EDOD and related regression line.

From this point on, attention shall be restricted to the linear dependence, Eq. (61), for simplicity. The general case, Eq. (58), will be considered later.

3.4. Different stages of evolution

The mere existence of a G-dwarf problem in different regions of the Galaxy (e.g. van den Bergh 1962, Schmidt 1963, H76, Prantzos 2003, Ferreras et al. 2003) and perhaps in all galaxies (Worthey et al. 1996, Henry and Worthey 1999) implies the EDOD cannot be fitted by a straight line as predicted by simple CBR models, but by a continuous broken line at most. To this aim, simple CBR models will be extended by allowing different flow regimes during different stages of evolution, and defined as simple multistage closed-(box+reservoir) (MCBR) models.

Accordingly, the flow κ is different in different stages while the equations of the model maintain their formal expression where variables and parameters are indexed by a letter U = I, II, III, ..., which denotes the stage under consideration. The cut $\zeta_{\rm O}$ could also be different in different stages but it will be kept equal to unity (i.e. flowing gas with same oxygen abundance with respect to the pre existing gas) to preserve the validity of the linear approximation. In general, the above restriction is viable for outflowing gas while it fails if the inflowing gas has different oxygen abundance with respect to the pre existing gas. Related effects will be discussed later.

With regard to the U-th stage, the TDOD, defined by Eq. (58), via Eq. (56) reads:

$$\psi_{\rm U}(\phi_{\rm U}) = \log\frac{{\rm d}s_{\rm U}}{[(s_{\rm U})_f - (s_{\rm U})_i]\,{\rm d}\phi_{\rm U}} \quad , \quad (72)$$

where $(s_{\rm U})_i$ and $(s_{\rm U})_f$ are the fractional star mass at the beginning and at the end of the U-th stage, respectively. The combination of Eqs. (53), (57), and (72), via Eqs. (61)-(63) yields:

$$\psi_{\rm U}(\phi_{\rm U}) = a_{\rm U}\phi_{\rm U} + b_{\rm U} \quad , \quad (73)$$

$$a_{\rm U} = -\frac{1}{\ln 10}\frac{(Z_{\rm O})_\odot}{\hat{p}''_{\rm U}} = -\frac{1}{\ln 10}\frac{(Z_{\rm O})_\odot}{\hat{p}_{\rm U}}(1+\kappa_{\rm U}) \ , \quad (74)$$

$$b_{\rm U} = \log\left[\frac{(\mu_{\rm U})_i}{(\mu_{\rm U})_i - (\mu_{\rm U})_f}(-\ln 10)a_{\rm U}\right] - a_{\rm U}(\phi_{\rm U})_i, \quad (75)$$

which are valid in the linear approximation.

The particularization of Eq. (68) to the U-th stage reads:

$$(\phi_{\rm U})_f - (\phi_{\rm U})_i = \frac{1}{\ln 10}\frac{1}{a_{\rm U}}\ln\frac{(\mu_{\rm U})_f}{(\mu_{\rm U})_i} \quad , \quad (76)$$

and the shifted TDOD intercept, via Eq. (75) translates into:

$$(b_{\rm U})_{\rm N} = b_{\rm U} + \log(C_{\rm U})_{\rm N} = \log\frac{(C_{\rm U})_{\rm N}(\mu_{\rm U})_i}{(\mu_{\rm U})_i - (\mu_{\rm U})_f} + \\ + \log\frac{(Z_{\rm O})_\odot}{\hat{p}''_{\rm U}} + \frac{1}{\ln 10}\frac{(Z_{\rm O})_\odot}{\hat{p}''_{\rm U}}(\phi_{\rm U})_i \quad , \quad (77)$$

and the combination of Eqs. (74), (76), and (77) yields,

$$(C_{\rm U})_{\rm N} = -\frac{1}{\ln 10}\frac{1}{a_{\rm U}}\exp_{10}[a_{\rm U}(\phi_{\rm U})_i + (b_{\rm U})_{\rm N}] \times \\ \times \{1 - \exp_{10}\{a_{\rm U}[(\phi_{\rm U})_f - (\phi_{\rm U})_i]\}\}, \quad (78)$$

which may be determined from the knowledge of the EDOD belonging to the U-th stage and related regression line. In general, different samples and/or different stages imply different values of the normalization constant that ensures continuity passing from the end of an assigned stage to the beginning of the next one.

3.5. Application to a special stellar system

For selected [O/H]-[Fe/H] relations, the EDOD related to the fs10 sample (taken as representative of ther inner Galactic halo) can be divided into four or three regions where the trend is linear to a good extent, as shown in Figs. 4 and 5. In the light of the model, each region corresponds to a different regime of chemical evolution, which may be related to a different regime of dynamical evolution. According to standard cosmological scenarios, overdensities decouple from the Hubble flow, expand, collapse and relax. The time scale of the process is proportional to the overdensity mass, which implies low-mass systems (e.g. dwarf spheroidal galaxies) formed long time ago while large-mass systems (e.g. cluster of galaxies) are still forming.

In any case, the system as a whole is poorly virialized in early times, when a high inflow of cosmological gas is expected (assembling stage). The inner and denser regions first virialize and a considerable gas flow is expected from more extended (e.g. proto-halo and proto-thick disk) to less extended (e.g. proto-bulge and proto-thin disk) subsystems (formation stage). The relaxed region grows in mass and size yielding a nearly virialized state where additional gas outflow via energy dissipation is expected from more extended to less extended subsystems (contraction phase). The system approaches a dynamical equilibrium configuration characterized by a considerable star mass fraction, where further gas outflow via energy dissipation is still expected from more extended to less extended subsystems (equilibrium stage). A major merger makes the system again poorly virialized (e.g. re-extending a bulge and/or re-thickening a thin disk) and the above mentioned process has to be repeated leaving aside the assembling stage. Different scenarios will be discussed in the next subsection.

Within the model, the gas and star mass fraction are left unchanged passing from a selected stage to the next one, which implies the validity of the following relations:

$$(X_{\rm U})_f = (X_{\rm V})_i \ , \ (X_{\rm A})_i = X_i \ , \ (X_{\rm E})_f = X_f \ , \tag{79a}$$

$$X = \mu, s, D \ , \quad {\rm U} = {\rm A}, {\rm F}, {\rm C} \ , \quad {\rm V} = {\rm F}, {\rm C}, {\rm E} \ , \tag{79b}$$

where X_i, X_f, are related to the whole evolution regardless of the stages. Accordingly, the mass conservation during the U-th stage may be expressed as:

$$\mu_{\rm U} + (1+\kappa_{\rm U}) s_{\rm U} = \mu_{\rm U} + s_{\rm U} + D_{\rm U} = \\ = (\mu_{\rm U})_i + (s_{\rm U})_i + (D_{\rm U})_i \ , \tag{80}$$

where the initial values are known via Eq. (79). The cut $(\zeta_{\rm O})_{\rm U}$ has also been kept equal to unity to preserve the linear approximation.

The regression line in an assigned region of the EDOD is defined by the slope $a_{\rm U}$ and the intercept $b_{\rm U}$ and the intersections between regression lines related to adjacent regions mark initial and final values of normalized oxygen abundance $(\phi_{\rm U})_i$ and $(\phi_{\rm U})_f$. The normalization constant $(C_{\rm U})_{\rm N}$ is determined via Eq. (78). The final value of the active gas mass fraction $(\mu_{\rm U})_f$ follows from Eq. (76).

The yield $\hat{p}$ and the lock α depend on the birth-rate stellar function. For a power-law stellar initial mass function, the EDOD in different Galactic environments is reproduced to a good extent from simple CBR models with the following output parameters (CM09):

$$\frac{\hat{p}}{(Z_{\rm O})_\odot} = 1.0340 \ , \tag{81a}$$

$$\alpha_{2.9} = 0.66604 \ , \qquad \alpha_{2.35} = 0.85360 \ , \tag{81b}$$

$$(\widetilde{m}_{\rm mf})_{2.9} = 0.44449 \ , \ (\widetilde{m}_{\rm mf})_{2.35} = 0.015436 \ , \tag{81c}$$

for an assumed solar oxygen abundance $(Z_{\rm O})_\odot = 0.0056$ where the indices relate to power-law exponents equal to 2.9 and 2.35, respectively. For further details refer to earlier attempts (C01, C07).

The flow $\kappa_{\rm U}$ is deduced from Eq. (74). The final star mass fraction $(s_{\rm U})_f$ and outflowed or inflowed gas mass fraction $(D_{\rm U})_f$ are determined from Eq. (80) particularized to the end of the U-th stage.

In the light of the model, the initial star mass fraction s_i results from the fractional mass in stars (including stellar remnants) with normalized oxygen abundance, $\phi < \phi_i$. The above value, though still uncertain at present, may be understimated to a good extent as $s_i = 0$. In addition, $D_i = 0$ without loss of generality, which implies $\mu_i = 1$.

The fractional mass of the box (with respect to the initial value) attains the maximum value at the end of A stage, where gas inflows into the box from the reservoir. The related value is $(\mu_{\rm A})_f + (s_{\rm A})_f$. The fractional mass in stars at the end of evolution, which coincides with the end of the E stage, is $(s_{\rm E})_f$. Accordingly, the mass ratio of the box at the end of evolution to the outflowed gas reads:

$$\frac{M_{\rm box}}{M_{\rm ofl}} = \frac{(\mu_{\rm E})_f + (s_{\rm E})_f}{(\mu_{\rm A})_f + (s_{\rm A})_f - (\mu_{\rm E})_f - (s_{\rm E})_f} \ , \tag{82}$$

provided the earlier stage A is in the inflow regime and the subsequent stages F, C, (or FC), E, are in the outflow regime, as it is the case for the EDOD and related TDOD under consideration.

With the above values of input parameters, the flow, the active gas mass fraction, the star mass fraction and the outflowed or inflowed gas mass fraction, at the end of each stage of evolution, can be computed. The results are listed in Table 6 for the EDOD related to the fs10 sample for [O/H]-[Fe/H] empirical relations deduced from the RB09 sample (top panel) and Fal09 sample, case SH1 (middle and bottom panel), see Fig. 4.

Table 6. Input parameters (deduced from the regression lines) $(\phi_{\rm U})_i$, $a_{\rm U}$, $b_{\rm U}$, and output parameters $\kappa_{\rm U}$, $(\mu_{\rm U})_f$, $(s_{\rm U})_f$, $(D_{\rm U})_f$, for simple MCBR models fitting to the EDOD related to the fs10 sample, for [O/H]-[Fe/H] empirical relations deduced from the RB09 sample (top panel) and Fal09 sample, case SH1 (middle and bottom panel). Four (A, F, C, E; top and middle panels) or three (A, FC, E; bottom panel) stages of evolution are considered, according to the linear trends exhibited by the EDOD (Fig. 4). Stages O before A and after E are not considered as no sample object lies within the corresponding metallicity range. Other input parameters are $(Z_{\rm O})_\odot = 0.0056$, $\hat{p}/(Z_{\rm O})_\odot = 1.0340$, $\mu_i = (\mu_{\rm O})_f = 1$, $s_i = (s_{\rm O})_f = 0$, $D_i = (D_{\rm O})_f = 0$, where the index O denotes the oxygen with regard to the solar abundance and stage O of evolution otherwise. The slope related to the stagnation regime is $a_{\rm U}(\kappa = 0) = -(1/\ln 10)[\hat{p}/(Z_{\rm O})_\odot] = -0.449075$. For further details refer to the text.

U	$(\phi_{\rm U})_i$	$a_{\rm U}$	$b_{\rm U}$	$\kappa_{\rm U}$	$(\mu_{\rm U})_f$	$(s_{\rm U})_f$	$(D_{\rm U})_f$
A	9.4624E−4	+1.1382E+2	−1.0567E−1	−2.7201E+2	9.9175E−0	3.2905E−2	−8.9504E−0
F	9.7001E−3	−2.0950E+0	+1.0188E−0	+3.9881E+0	7.7178E−0	4.7391E−1	−7.1917E−0
C	6.1687E−2	−7.3565E+0	+1.3433E−0	+1.6515E+1	4.5710E−1	8.8844E−1	−3.4554E−1
E	2.2854E−1	−2.2569E+0	+1.7784E−1	+4.3735E+0	3.5961E−2	9.6681E−1	−2.7737E−3
O	7.1779E−1						
A	3.1623E−4	+7.9432E+1	+2.7571E−1	−1.9012E+2	3.6714E−0	1.4125E−2	−2.6855E−0
F	7.4271E−3	−3.8855E+0	+8.9453E−1	+8.2913E+0	1.2551E−0	2.7531E−1	−5.3043E−1
C	1.2740E−1	−2.6460E+0	+7.3661E−1	+5.3000E+0	5.4973E−2	4.6581E−1	+4.7922E−1
E	6.4083E−1	−5.3661E−1	−6.1514E−1	+2.7764E−1	2.4384E−3	5.0693E−1	+4.9063E−1
O	3.1623E−0						
A	3.1623E−4	+7.9432E+1	+2.7571E−1	−1.9012E+2	3.2209E−0	1.1743E−2	−2.2327E−0
FC	6.7114E−3	−2.8643E+0	+8.2804E−1	+5.8196E+0	5.6405E−2	4.7577E−1	+4.6782E−1
E	6.2002E−1	−5.3661E−1	−6.1514E−1	+2.7764E−1	2.4384E−3	5.1801E−1	+4.7955E−1
O	3.1623E−0						

With regard to the bottom panel, stages F and C are merged into a single one, FC.

In the former case (top panel), where the empirical [O/H]-[Fe/H] relation has been determined using the LTE approximation (RB09), the mass of the box is increased by a factor of about 10 at the end of the A stage, and is reduced to about the initial value at the end of the E stage. The mass ratio $M_{\rm box}/M_{\rm ofl}$ equals to about 0.11 via Eq. (82).

In the latter case (middle and bottom panel), where the empirical [O/H]-[Fe/H] relation has been determined relaxing the LTE approximation (Fal09), the mass of the box is increased by a factor of about 3-4 at the end of the A stage and is reduced to about one half the initial value at the end of the E stage. The mass ratio $M_{\rm box}/M_{\rm ofl}$ equals to about 0.16-0.19 via Eq. (82).

In any case, the initial mass of the box at the beginning of the A stage (proto-inner halo) is comparable to the mass of the box at the end of the E stage (present inner halo).

3.6. Departure from linear approximation

As outlined in Subsection 3.1, the validity of the linear approximation implies values of the cut very close to unity i.e. nearly equal oxygen abundance within the flowing and pre existing gas. The above restriction is less plausible for the gas inflowing from intergalactic medium where metal abundance (at any epoch) is expected to be lower than galaxies. On the other hand, it is viable for gas outflowing to interstellar medium where metal abundance is expected to maintain the same or be slightly increased with respect to pre existing gas. An inspection of Fig. 5 shows a large gas inflow during the A stage and consistent or a moderate gas outflow during the F, C, (or FC) and E stage. Accordingly, the strongest violation to the linear approximation is expected to occur at the beginning of evolution and attention shall be focused on the A stage.

In dealing with the general case, nonlinear interpolation to the data shall not be exploited to save space and avoid cumbersome formulation. A viable alternative consists in considering a family of TDOD curves, Eq. (58), including the regression line and passing through the zero point $(0, b_{\rm N})$ and the ending point (ϕ_f, ψ_f) within the domain $\phi_i \leq \phi \leq \phi_f$ where $\psi_f = \psi(\phi_f) = a\phi_f + b_{\rm N}$. Then, the value of the flow κ may be calculated for an assigned cut $\zeta_{\rm O}$ and the TDOD may be determined using Eqs. (25), (58), (59) and (69).

With regard to RB09 sample restricted to the A stage, the TDOD for $\zeta_{\rm O} = 0.0, 0.1, ..., 1.2$, is plotted in Fig. 6 and compared to the related EDOD. In particular, $\zeta_{\rm O} = 0$ corresponds to a primordial (metal free) composition. Some parameters are listed in Table 7.

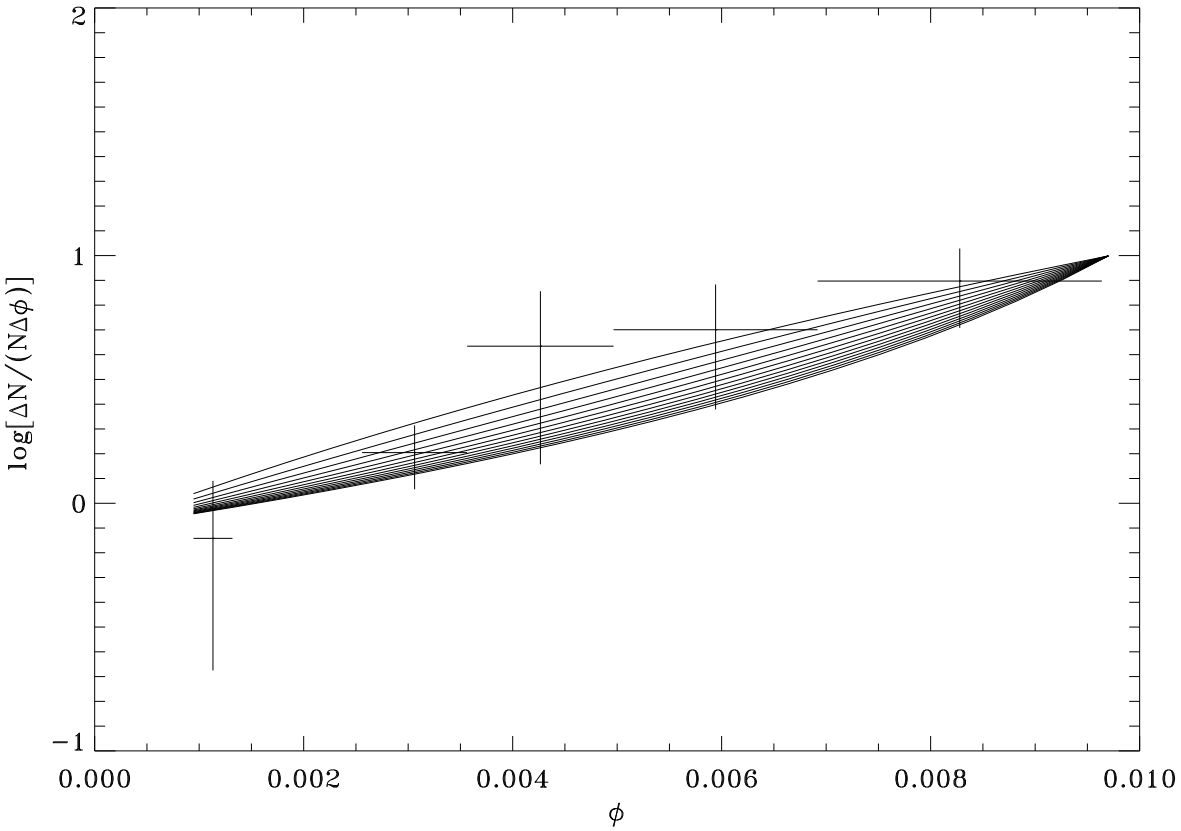

Fig. 6. *Comparison between the empirical (EDOD), deduced from the FB09 sample restricted to the A stage, and theoretical (TDOD) differential oxygen abundance distribution defined by the family of curves including the regression line and passing through the zero point* $(0, b_{\rm N})$ *and the ending point* (ϕ_f, ψ_f) *where* $\psi_f = a\phi_f + b_{\rm N}$. *Curves correspond (from bottom to top) to cut values* $\zeta_{\rm O} = 0.0, 0.1, ..., 1.2$. *In general, for varying cut* $(\zeta_{\rm O})_{\rm min} \leq \zeta_{\rm O} \leq (\zeta_{\rm O})_{\rm max}$, *the TDOD lies within the region bounded by the curves* $\zeta_{\rm O} = (\zeta_{\rm O})_{\rm min}$ *and* $\zeta_{\rm O} = (\zeta_{\rm O})_{\rm max}$.

Table 7. Values of the cut $\zeta_{\rm O}$, the flow κ, the fractional flow κ/κ_1, $\kappa_1 = \kappa(\zeta_{\rm O} = 1)$, the fractional mass μ_f/μ_i, the parameter c, and the normalization constant $C_{\rm N}$ for the family of theoretical differential oxygen abundance distributions plotted in Fig. 6 with regard to FB09 sample restricted to the A stage. For further details refer to the text.

$\zeta_{\rm O}$	$-\kappa$	κ/κ_1	μ_f/μ_i	c	$C_{\rm N}$
0.0	7.6841E+1	2.8286E−1	3.2897E+0	+7.4419E+1	2.6271E−2
0.1	8.3187E+1	3.0582E−1	3.4991E+0	+7.2416E+1	2.6649E−2
0.2	9.0496E+1	3.3269E−1	3.7461E+0	+7.0025E+1	2.7076E−2
0.3	9.9154E+1	3.6452E−1	4.0409E+0	+6.7134E+1	2.7559E−2
0.4	1.0955E+2	4.0276E−1	4.3976E+0	+6.3580E+1	2.8112E−2
0.5	1.2226E+2	4.4946E−1	4.8360E+0	+5.9129E+1	2.8749E−2
0.6	1.3809E+2	5.0765E−1	5.3843E+0	+5.3427E+1	2.9491E−2
0.7	1.5827E+2	5.8185E−1	6.0842E+0	+4.5929E+1	3.0263E−2
0.8	1.8476E+2	6.7923E−1	6.9985E+0	+3.5747E+1	3.1402E−2
0.9	2.2078E+2	8.1166E−1	8.2747E+0	+2.1363E+1	3.2655E−2
1.0	2.7201E+2	1	9.9189E+0	+1.1200E−2	3.4190E−2
1.1	3.4924E+2	1.2839E+0	1.2332E+1	−3.3763E+1	3.6101E−2
1.2	4.7508E+2	1.7465E+0	1.5860E+1	−9.1877E+1	3.8520E−2

An inspection of Fig. 6 shows that in all cases, including both the lower and higher inflowing gas oxygen abundance with respect to the pre existing gas, fit to the data. More specifically, lower flows κ, implying lower fractional mass ratios μ_f/μ_i, are needed for lower cuts $\zeta_{\rm O}$, and vice versa, as shown in Table 7. In particular, the TDOD fits to the EDOD for cuts within the range $0 \leq \zeta_{\rm O} \leq 1.2$, corresponding to flows $-76.941 \geq \kappa \geq -475.08$, and fractional mass ratios $3.2897 \leq \mu_f/\mu_i \leq 15.8596$. It can also be seen that the normalization constant $C_{\rm N}$ is only slightly changed by a few percent with respect to the linear approximation $\zeta_{\rm O} = 1$.

In the general case of a varying oxygen abundance within the flowing gas i.e. varying cut $(\zeta_{\rm O})_{\rm min} \leq \zeta_{\rm O} \leq (\zeta_{\rm O})_{\rm max}$, the TDOD belonging to the family of curves passing through the zero point $(0, b_{\rm N})$ and the ending point (ϕ_f, ψ_f) intersects all curves characterized by constant $\zeta_{\rm O}$ in the range under consideration, lying within the region bounded by the curves where $\zeta_{\rm O} = (\zeta_{\rm O})_{\rm min}$ and $\zeta_{\rm O} = (\zeta_{\rm O})_{\rm max}$. As shown in Fig. 6, the TDOD fits to the EDOD even if the cut $\zeta_{\rm O}$ varies within the range $0 \leq (\zeta_{\rm O})_{\rm min} \leq \zeta_{\rm O} \leq (\zeta_{\rm O})_{\rm max} \leq 1.2$.

Table 8. Values of active gas, long-lived stars and flowing gas mass fractions at the end of each stage for the extreme situations of inflowing gas with equal ($\zeta_{\rm O} = 1$, upper lines) and null ($\zeta_{\rm O} = 0$, lower lines) oxygen abundance with respect to the pre existing gas, in connection with RB09 (top) and Fal09 (middle, 4 stages; bottom, 3 stages) samples.

U	$(\mu_{\rm U})_f$	$(s_{\rm U})_f$	$(D_{\rm U})_f$
A	9.9189E−0	3.2910E−2	−8.5518E−0
	3.2897E−0	3.0151E−2	−2.3199E−0
F	7.7188E−0	4.7398E−1	−7.1928E−0
	2.5600E−0	1.7644E−1	−1.7365E−0
C	4.5716E−1	8.8856E−1	−3.4579E−1
	1.5162E−1	3.1394E−1	+5.3444E−1
E	3.5966E−2	9.6695E−1	−2.9114E−3
	1.1929E−2	3.3994E−1	+6.4814E−1
A	3.6711E−0	1.4125E−2	−2.6853E−0
	1.9216E−0	1.3558E−2	−9.3520E−1
F	1.2550E−0	2.7529E−1	−5.3031E−1
	6.5694E−1	1.5026E−1	+1.9280E−1
C	5.4969E−2	4.6577E−1	+4.7926E−1
	2.5773E−2	3.5000E−1	+7.2125E−1
E	2.4383E−3	5.0689E−1	+4.9067E−1
	1.2763E−3	2.7149E−1	+7.2723E−1
A	3.2207E−0	1.1743E−2	−2.2325E−0
	1.7998E−0	1.1422E−2	−8.1127E−1
FC	5.6401E−2	4.7574E−1	+4.6786E−1
	3.1519E−2	2.7072E−1	+6.9776E−1
E	2.4383E−3	5.1798E−1	+4.7958E−1
	1.3626E−3	2.9432E−1	+7.0431E−1

Values of active gas, long-lived star and flowing gas mass fractions at the end of each stage are listed in Table 8 for the extreme situations of inflowing gas with equal ($\zeta_{\rm O} = 1$, upper lines) and null ($\zeta_{\rm O} = 0$, lower lines) oxygen abundance with respect to the pre existing gas during the A stage. The former case corresponds to the linear approximation ($c << 1$) yielding results slightly different (as expected) from their counterparts listed on Table 6 where a linear dependence is assumed explicitly ($c = 0$). Values of the remaining parameters can be read in Tables 6 (initial and final normalized oxygen abundance, regression line slope and intercept) and 7 (flow). An inspection of Table 8 discloses that both the active gas and long-lived star mass fraction are lowered by a factor of about 2-3, passing from the unit cut $\zeta_{\rm O} = 1$ to the null cut $\zeta_{\rm O} = 0$ and the outflowing gas mass fraction at the end of evolution is enhanced.

3.7. Discussion

Though TDODs calculated using simple MCBR models of chemical evolution fit to EDODs with different linear trends in different regions, as shown in Fig. 5, the application to the inner Galactic halo still remains speculative in absence of further improvement. The main reasons are outlined below.

According to the results listed in Table 6 and plotted in Fig. 5, the EDOD deduced for the inner halo exhibits a positive slope (implying gas inflow) at the initial stage A and negative slope (implying gas outflow) at the subsequent stages F, C (or FC), E, within the errors ($\mp\sigma_a$). Though a similar trend has been inferred for globular clusters (C07), bulge (C07), and disk (Caimmi 2008) data, the inner halo EDOD should be redetermined using a homogeneous, unbiased and well populated sample. Direct oxygen abundance determinations (Ramirez et al. 2007) where different methods yield consistent results or, at least, a [O/H]-[Fe/H] relation which attains general consensus, would also be effective for improving the results.

Though the assumption of null star mass fraction holds to a good extent for the starting configuration, the presence of stars with lower metallicity with respect to sample objects, [Fe/H] < -4.2, has still to be considered. This extremely low metallicity has currently been detected in about a dozen of stars down to [Fe/H] ≈ -5.4 (e.g. Beers and Christlieb 2005). Basing on theoretical arguments, a lower limit oxygen abundance in Pop II stars has been determined as [O/H] $= -3.05 \mp 0.20$ (Bromm and Loeb 2003) where the earlier nucleosynthesis comes from more massive Pop III stars.

If the transition from the latter to the former population was not instantaneous, and coeval Pop III and Pop II stars were generated (Smith et al. 2009), then the stellar initial mass function can no longer be considered as universal in time for Pop II stars. Accordingly, model evolution must be started after the last Pop III star has undergone supernova explo-

sion, which has been assumed to take place when the metal abundance is [Fe/H] = −4.2. In absence (to the knowledge of the author) of a reliable estimate of the mass fraction in stars and stellar remnants with initial metal abundance, [Fe/H] < −4.2, a null value has been assigned.

In the light of accretion scenarios of galaxy formation, the (initially) inflowing gas can be primordial (metal free) for low-mass overdensities which form earlier, and metal enriched for high-mass overdensities which form later.

According to the classical hot-mode, the baryonic Hubble flow falls into a dark matter potential well, radially and isotropically to an acceptable extent, and is shock-heated until it attains quasi hydrostatic equilibrium. Energy dissipation in the inner and denser regions makes the gas collapse to a centrifugally supported disk where a star formation occurs (e.g. Rees and Ostriker 1977, White and Rees 1978, White and Frenk 1991).

According to the cold-mode, the baryonic Hubble flow is substructured into filaments and gas accretion occurs via cold streams where a substantial gas mass fraction never attains hydrostatic equilibrium (e.g. Keres et al. 2005, Dekel et al. 2009, van de Voort et al. 2011, Davè et al. 2011).

The hot-mode dominates at low redshifts ($0 \leq z \lesssim 3$) in groups and cluster environments, while the cold mode dominates at high redshifts ($z \gtrsim 3$) and in low-density environments today. Related mass ranges are $M_{\rm gal} \gtrsim M^*_{\rm gal}$ and $M_{\rm gal} \lesssim M^*_{\rm gal}$, respectively, for baryons, and $M_{\rm h} \gtrsim M^*_{\rm h}$ and $M_{\rm h} \lesssim M^*_{\rm h}$, respectively, for the dark matter where $M^*_{\rm gal} \approx 2\,10^{10} m_\odot$ and $M^*_{\rm h} \approx 2.5\,10^{11} m_\odot$ (Keres et al. 2005).

In the light of merger scenarios of galaxy formation, the inflowing gas is necessarily related to wet mergers, where the metal abundance is determined by the past history of the accreted system. Wet mergers dominate below a stellar mass threshold, $M_* \lesssim M_{*T} \approx 3\,10^{10} m_\odot$, dry mergers dominate above, $M_* \gtrsim M_{*T}$, major dry mergers dominate above a stellar mass threshold, $M_* \gtrsim M_{*M} \approx 2\,10^{11} m_\odot$ (Bernardi et al. 2011), and galaxies form inside a hierarchically growing system of dark matter haloes (Cole et al. 2000, De Lucia et al. 2006, Shankar et al. 2011).

The above mentioned scenarios of the galaxy formation also indicate a need for strong outflow from the system. These outflows are likely to escape galactic potential in low-mass haloes (e.g. Dekel and Silk 1986) while, in more massive objects, most of the ejected material is able to flow back to form stars in galaxies (e.g. Oppenheimer et al. 2010, Lehner and Howk 2011). Accordingly, the initial mass of the proto-Galaxy plays a crucial role in the evolution. If the proto-halo and the proto-bulge had a common origin regardless of the scenario of the galaxy formation, it is conceivable that halo stars formed first when the gas component was largely unrelaxed, and bulge stars formed soon after when the gas component was nearly relaxed (e.g. Minniti 1996).

In this view, gas rapidly settles from a larger volume (halo) to a smaller volume (bulge) or, in other words, outflows from a spherical homeoid bounded by halo and bulge surface to the inner sphere filled by the bulge. On the other hand, the gas lost from halo planetary nebulae may be dispersed outside to enrich the intergalactic medium. According to recent investigations, the Galactic bulge is made of an inner component which exhibits a bar-like kinematics and metal-rich population, and an outer component which exhibits a spheroid kinematics and a metal-poor population (Babusiaux et al. 2010). If the inner halo and the outer bulge had a common origin, in the sense specified above, then a similar specific angular momentum distribution would be expected for the inner halo and the outer bulge.

In this view, the mass ratio of the box at the end of evolution to the gas outflowed from the box into the reservoir during the evolution, $M_{\rm box}/M_{\rm ofl}$, expressed by Eq. (82), should reproduce the mass ratio of (inner) halo to (outer) bulge, as:

$$\frac{(M_{\rm H})_{\rm inn}}{(M_{\rm B})_{\rm out}} = \frac{(M_{\rm H})_{\rm inn}/M_{\rm H}}{(M_{\rm B})_{\rm out}/M_{\rm B}} \frac{M_{\rm H}}{M_{\rm B}} \quad , \qquad (83)$$

which is equivalent to:

$$\frac{(M_{\rm H})_{\rm inn}}{M_{\rm H}} = \frac{(M_{\rm H})_{\rm inn}/(M_{\rm B})_{\rm out}}{M_{\rm H}/M_{\rm B}} \frac{(M_{\rm B})_{\rm out}}{M_{\rm B}} \quad , \qquad (84)$$

where the indices, "inn" and "out", denote the inner and outer component, respectively, H the halo, and B the bulge. The inner halo to the outer bulge mass ratio, deduced from the results listed in Table 8, is $(M_{\rm H})_{\rm inn}/(M_{\rm B})_{\rm out} = (s_{\rm E})_f/(\mu_{\rm A})_f \approx 0.10$-$0.16$. The halo to bulge mass ratio is currently estimated as $M_{\rm H}/M_{\rm B} \approx 0.05$-$0.10$. Then, simple MCBR models considered here yield, in the case under discussion, an inner halo fractional mass (normalized to the halo) which is comparable to, or exceeding by a factor up to about 3, the outer bulge fractional mass (normalized to the bulge). On the other hand, quantitative results cannot be expected for the above mentioned reasons. In conclusion, the (inner) halo to (outer) bulge mass ratio appears to be an additional output parameter provided by simple MCBR models of chemical evolution, with regard to the inner Galactic halo.

According to recent results (Jofré and Weiss 2011), the inner Galactic halo dominant population is coeval, implying a rapid collapse of and rapid star formation within the proto-halo. In addition, *in situ* star formation likely represents the solution to the long-standing failure of pure accretion-based models to reproduce the observed properties of stellar haloes around disk galaxies (Font et al. 2011). The presence of bluer i.e. younger population results from accretion of smaller subunits (mainly dwarf spheroidal galaxies) after the formation of the inner halo. In fact, globular clusters belonging to the inner and outer halo are usually classified as "old halo" and "young halo", respectively (e.g. Mackey and van den Bergh 2005), where old halo globular clusters

are coeval to old halo field stars (Jofré and Weiss 2011). A (inner) halo - (metal-poor) bulge collapse can be inferred by comparison of related specific angular momentum distributions (Wise and Gilmore 1992), which implies the bulge formation is subsequent to inner halo formation, and then the (metal-poor) bulge may be considered as a reservoir for the outflowing gas, in the sense specified by the model.

4. CONCLUSION

Under the assumption that two samples of halo stars, RN91 and H V, are equally representative of the inner Galactic halo within the metallicity range $-3.0 \leq$ [Fe/H] ≤ -2.8 a fictitious sample fs10 has been built up and taken as representative of the inner Galactic halo within the metallicity range $-4.2 \leq$ [Fe/H] $\leq +0.2$. The related differential empirical oxygen abundance distribution (EDOD) has been established using different [O/H]-[Fe/H] empirical relations deduced from different samples (RB09, Fal09, Sal09) where different methods have been exploited for determining the oxygen abundance.

More precisely, the EDOD has been deduced from the fs10 sample by use of two alternative [O/H]-[Fe/H] empirical relations: one, determined from the RB09 sample in presence of local thermodynamical equilibrium (LTE) approximation (RB09), and the other, determined from the Fal09 sample in absence of LTE approximation with due account taken of the inelastic collisions via neutral H atoms SH1 (Fal09, $S_{\rm H} = 1$) as shown in Fig. 3.

A linear trend has been exhibited by related EDODs within three or four regions, as shown in Fig. 4, and the slope and intercept estimators of corresponding regression lines have been determined together with their dispersions, using different interpolation methods as shown in Table 2 with regard to bisector regression. It has been pointed out that the earlier trend, characterized by a positive slope, is a signature of a G-dwarf problem.

The main uncertainties on the EDOD have been recognized as related to: (1) biases on the RN91 and H V samples due to selection effects towards sufficiently low ([Fe/H] < -4.2) and sufficiently high ([Fe/H] > -2.8) metal abundance (H V) and disk contamination for [Fe/H] > -2.0 (RN91; H V), and (2) lack of clear indications on a recommended method for determining oxygen abundance, as shown in Table 1 and in Fig. 1 for 11 stars in common among the RB09 and the Fal09 sample.

Fitting a theoretical differential oxygen abundance distribution (TDOD) to the EDOD discussed above has needed an extension of simple closed-box (CB) models of chemical evolution on two respects. First, the system has been conceived as made of a box and a reservoir, where the following processes have been allowed: the gas outflow from the box into the reservoir (H76), moderate gas inflow (C07), steady and strong gas inflow (current paper) into the box from the reservoir. Simple closed-(box+reservoir) (CBR) models have exhibited mass conservation within the system (box+reservoir) while it has been violated within a single subsystem (box or reservoir). Second, the history of the system has been conceived as a succession of a different stages characterized by different outflow or inflow rate.

In the special case of flowing gas with equal oxygen abundance with respect to the pre existing gas, $\zeta_{\rm O} = 1$, simple multistage closed-(box+reservoir) (MCBR) models have been found to yield TDODs in the form of continuous broken lines, which can fit to related EDODs. In the general case $\zeta_{\rm O} \neq 1$ the segments of the broken line are expected to be slightly curved downwards or upwards depending whether $0 \leq \zeta_{\rm O} < 1$ or $\zeta_{\rm O} > 1$, respectively, as depicted in Fig. 6 for the earlier stage A.

An application of MCBR models to a special stellar system resembling the inner Galactic halo has been made with fiducial values of input parameters which cannot be deduced from the EDOD. The metal abundance at the beginning and at the end of each stage, have been inferred from the intersection of regression lines fitting to adjacent regions of the EDOD, as shown in Fig. 5. The mass ratio of the box at the end of evolution to the gas outflowed from the box into the reservoir through the evolution, has been determined via Eq. (82) as $M_{\rm box}/M_{\rm ofl} \approx 0.11$ for a [O/H]-[Fe/H] empirical relation deduced from the RB09 sample in presence of LTE approximation (RB09), and $M_{\rm box}/M_{\rm ofl} \approx$ 0.16-0.19 for a [O/H]-[Fe/H] empirical relation deduced from the Fal09 sample in absence of LTE approximation with due account taken of the inelastic collisions via neutral H atoms, SH1 (Fal09, $S_{\rm H} = 1$), with regard to four and three stages of evolution, respectively.

For current estimates of the halo-to-bulge mass ratio $M_{\rm halo}/M_{\rm bulge} \approx$ 0.05-0.10 the inner halo fractional mass (normalized to the halo) has been found to be comparable with, or exceeding by a factor up to 3, the metal-poor bulge fractional mass (normalized to the bulge). On the other hand, it has been considered that quantitative predictions cannot be made for the Galaxy unless complete and unbiased samples of the inner Galactic halo are available, and discrepancies among [O/H]-[Fe/H] empirical relations related to different samples and different methods are removed.

Acknowledgements – The author is indebted to an anonymous referee for critical comments which improved an earlier version of the manuscript.

REFERENCES

Asplund, M., Grevesse, N., Sauval, A. J., Scott, P.: 2009, *Ann. Rev. Astron. Astrophys.*, **47**, 481.
Babusiaux, C., Gomez, A, Hill, V. et al.: 2007, *Astron. Astrophys.*, **519**, A77.

Barbuy, B., Nissen, P. E.: 2001, Peterson, R., Spite, F. (eds.), Proceedings of Oxygen abundances in Old Stars and Implications for Nucleosynthesis and Cosmology (IAU Joint Discussion 8). *New Astron. Rev.*, **45**, 509.
Beers, T. C., Christlieb, D.: 2005, *Annu. Rev. Astron. Astrophys.*, **43**, 531.
Bernardi, M., Roche, N., Shankar, F., Sheth, R. K.: 2011, *Mon. Not. R. Astron. Soc.*, **12**, L6.
Bouché, N., Dekel, A., Genzel, R. et al.: 2010, *Astrophys. J.*, **718**, 1001.
Bromm, V., Loeb, A.: 2003, *Nature*, **425**, 812.
Caimmi, R.: 2000, *Astron. Nachr.*, **321**, 323. (C00).
Caimmi, R.: 2001a, *Astron. Nachr.*, **322**, 65. (C00, erratum).
Caimmi, R.: 2001b, *Astron. Nachr.*, **322**, 241. (C01).
Caimmi, R.: 2007, *New Astron.*, **12**, 289. (C07).
Caimmi, R.: 2008, *New Astron.*, **13**, 314.
Caimmi, R.: 2011a, *New Astron.*, **16**, 337.
Caimmi, R.: 2011b, arXiv:1111.2680.
Caimmi, R., Milanese, E.: 2009, *Astrophys. Space Sci.*, **323**, 147. (CM09).
Carollo, D., Beers, T. C., Lee, Y. S.: et al.: 2007, *Nature*, **318**, 1020.
Carollo, D., Beers, T. C., Chiba, M.: et al.: 2010, *Astrophys. J.*, **712**, 692.
Cole, S., Lacey, C. G., Bergh, C. M., Frenk, C. S.: 2000, *Mon. Not. R. Astron. Soc.*, **319**, 168.
Davé, R., Finlator, K., Oppenheimer, B. D.: 2011, *Mon. Not. R. Astron. Soc.*, in press.
De Angeli, F., Piotto, G., Cassisi, S. et al.: 2005, *Astron. J.*, **130**, 116.
Dekel, A., Silk, J.: 1986, *Astrophys. J.*, **303**, 39.
Dekel, A., Bimboim, Y., Engel, G. et al.: 2009, *Nature*, **457**, 451.
De Lucia, G., Springel, V., White, S. D. M. et al.: 2006, *Mon. Not. R. Astron. Soc.*, **366**, 499.
Dutton, A. A., van den Bosh, F. C., Dekel, A.: 2010, *Mon. Not. R. Astron. Soc.*, **405**, 1690.
Fabbian, D., Nissen, P. E., Asplund, M. et al.: 2009, *Astron. Astrophys.*, **500**, 1143. (Fal09).
Feigelson, E. D., Babu, G. J.: 1992, *Astrophys. J.*, **397**, 55.
Ferreras, I., Wyse, R. F. G., Silk, J.: 1999, *Mon. Not. R. Astron. Soc.*, **345**, 1381.
Finlator, K., Davé, R.: 2008, *Mon. Not. R. Astron. Soc.*, **385**, 2181.
Font, A. S., McCarthy, I. G., Crein, R. A. et al.: 2011, *Mon. Not. R. Astron. Soc.*, **416**, 2802.
Guo, Q., White, S. D. M.: 2008, *Mon. Not. R. Astron. Soc.*, **384**, 2.
Hartwick, F. D. A.: 1976, *Astrophys. J.*, **209**, 418. (H76).
Haywood, M.: 2001, *Mon. Not. R. Astron. Soc.*, **325**, 1365.
Henry, R. B. C., Worthey, G.: 1999, *Publ. Astron. Soc. Pac.*, **111**, 919.
Isobe, T., Feigelson, E. D., Akritas, M. G., Babu, G. J.: 1990, *Astrophys. J.*, **364**, 104.
Jofré, P., Weiss, A.: 2011, *Astron. Astrophys.*, **533**, A59.
Katz, N., Weimberg, D. H., Hernquist, L.: 1996, *Astrophys. J. Suppl. Series*, **105**, 19.
Keres, D., Katz, N., Weimberg, D. H., Davé, R.: 2005, *Mon. Not. R. Astron. Soc.*, **363**, 2.
Lehner, N., Howk, J. C.: 2011, *Science*, **334**, 955.
Li, H. N., Christlieb, N., Schörck, T. et al.: 2010, *Astron. Astrophys.*, **521**, A10.
Mackey, A. D., van den Bergh, S.: 2005, *Mon. Not. R. Astron. Soc.*, **360**, 631.
Malinie, G., Hartmann, D. H., Clayton, D. D., Mathews, G. J.: 1993, *Astrophys. J.*, **413**, 633.
Marín-Franch, A., Aparicio, A., Piotto, G. et al.: 2009, *Astrophys. J.*, **694**, 1498.
Melendez, J., Asplund, M., Alves-Brito, A. et al.: 2008, *Astron. Astrophys.*, **484**, L21.
Minniti, D.: 1996, *Astrophys. J.*, **459**, 175.
Nissen, P. E., Schuster, W. J.: 2010, *Astron. Astrophys.*, **511**, L10.
Oppenheimer, R. D., Davé, R., Keres, D. et al.: 2010, *Mon. Not. R. Astron. Soc.*, **406**, 2325.
Pagel, B. E. J.: 1989, The G-dwarf Problem and Radio-active Cosmochronology. In: Beckman J.E., Pagel B.E.J. (eds.) Evolutionary Phenomena in Galaxies, Cambridge University Press, Cambridge, 201.
Pagel, B. E. J., Patchett, B. E.: 1975, *Mon. Not. R. Astron. Soc.*, **172**, 13.
Prantzos, N.: 2003, *Astron. Astrophys.*, **404**, 211.
Prantzos, N.: 2007, The Chemical Evolution of the Milky Way in a cosmological context, EAS Publications Series, **24**, 3.
Prantzos, N.: 2010, Topics of Galactic Chemical Evolution, 11th Symposium on Nuclei in the Cosmos, Heidelberg, published online at htpp://pos.sissa.it/cgi-bin/reader/conf.cgi?confid=100.
Ramirez, I., Allende Prieto, C., Lambert, D. L.: 2007, *Astron. Astrophys.*, **465**, 271.
Rees, M. J., Ostriker, J. P.: 1977, *Mon. Not. R. Astron. Soc.*, **179**, 541.
Rich, J. A., Boesgaard, A. M.: 2009, *Astrophys. J.*, **701**, 519. (RB09).
Rocha-Pinto, H. J., Maciel, W. J.: 1996, *Mon. Not. R. Astron. Soc.*, **279**, 447.
Ryan, S. G., Norris, J. E.: 1991, *Astron. J.*, **101**, 1865. (RN91).
Sadler, E. M., Rich, R. M., Terndrup, D. M.: 1996, *Astron. J.*, **112**, 171.
Salaris, M., Weiss, A.: 2002, *Astron. Astrophys.*, **388**, 492.
Schaye, J., Dalla Vecchia, C., Booth, C. M. et al.: 2010, *Mon. Not. R. Astron. Soc.*, **402**, 1536.
Schmidt, M.: 1959, *Astrophys. J.*, **129**, 243.
Schmidt, M.: 1963, *Astrophys. J.*, **137**, 758.
Schmidt, S. J., Wallerstein, G., Woolf, V. M., Bean, J. L.: 2009, *Publ. Astron. Soc. Pac.*, **121**, 1083. (Sal09).
Schönrich, R., Asplund, M., Casagrande, L.: 2011, *Mon. Not. R. Astron. Soc.*, **415**, 3807.
Schörck, T., Christlieb, N., Cohen, J. G. et al.: 2009, *Astron. Astrophys.*, **507**, 817. (H V).
Schuster, W. J., Moitinho, A., Mírquez, A., Parrao, L., Covarrubias, E.: 2006, *Astron. Astrophys.*, **445**, 939.
Shankar, F., Marulli, F., Bernardi, M. et al.: 2011, arxiv1105.6043.
Smith, B. D., Tuck, M. J., Sigurdsson, S. et al.: 2009, *Astrophys. J.*, **691**, 441.
Truran, J. W., Cameron, A. G. W.: 1971, *Astrophys. Space Sci.*, **14**, 179.
van den Bergh, S.: 1962, *Astrophys. J.*, **67**, 486.

van de Voort, F., Schaye, J., Booth, C. M. et al.: 2011, *Mon. Not. R. Astron. Soc.*, **414**, 2458.
Wang, B., Silk, J.: 1993, *Astrophys. J.*, **406**, 580.
White, S. D. M., Rees, M. J.: 1978, *Mon. Not. R. Astron. Soc.*, **183**, 341.
White, S. D. M., Frenk, C. S.: 1991, *Astrophys. J.*, **379**, 52.
Worthey, G., Dorman, B., Jones, L. A.: 1996, *Astron. J.*, **112**, 948.
Wyse, R. F. G., Gilmore, G.: 1992, *Astron. J.*, **104**, 144.

APPENDIX

A1 Steady inflow regime

The special case of steady inflow regime may be of particular relevance, as star-forming galaxies in hydrodynamic simulations are usually seen to lie near a steady state where gas subtracted by star formation is balanced by inflowing gas (e.g. Finlator and Davé 2008, Dutton et al. 2010, Davé et al. 2011b). For this reason, further attention shall be deserved to steady inflow regime, where $\kappa = -1$.

The gas mass within the box maintains constant, $\mathrm{d}M_g/\,\mathrm{d}t = 0$, and the substitution of Eqs. (11)-(13) into (10) yields:

$$\frac{\mathrm{d}M_{\mathrm{gO}}}{\mathrm{d}t} = [-Z_{\mathrm{O}}\alpha(1-\zeta_{\mathrm{O}}) + (1-Z)\hat{p}\alpha]\,\frac{\mathrm{d}M_{\mathrm{S}}}{\mathrm{d}t}; \quad (85)$$

dividing by the initial mass M_0 and using Eqs. (14), (16), Eq. (85) reads:

$$\mu_i \frac{\mathrm{d}Z_{\mathrm{O}}}{\mathrm{d}t} = [-Z_{\mathrm{O}}(1-\zeta_{\mathrm{O}}) + (1-Z)\hat{p}]\,\frac{\mathrm{d}s}{\mathrm{d}t} \quad , \quad (86)$$

where $\mu = \mathrm{const} = \mu_i$. The elimination of the temporal dependence yields:

$$\frac{\mathrm{d}Z_{\mathrm{O}}}{(1-Z) - Z_{\mathrm{O}}\hat{p}^{-1}(1-\zeta_{\mathrm{O}})} = \frac{\hat{p}\,\mathrm{d}s}{\mu_i} \quad , \quad (87)$$

and the comparison with the general case, Eqs. (19)-(20), shows the following:

$$\lim_{\kappa\to-1}\left(-\frac{1}{1+\kappa}\frac{\mathrm{d}\mu}{\mu}\right) = \frac{\mathrm{d}s}{\mu_i} \quad , \quad (88)$$

or:

$$\lim_{\kappa\to-1}\left(-\frac{\hat{p}''\,\mathrm{d}\mu}{\mu}\right) = \frac{\hat{p}\,\mathrm{d}s}{\mu_i} \quad , \quad (89)$$

in integral form:

$$\lim_{\kappa\to-1}\left(-\hat{p}''\ln\frac{\mu}{\mu_i}\right) = \frac{\hat{p}}{\mu_i}(s-s_i) \quad , \quad (90)$$

where $\mu \to \mu_i$ as $\kappa \to -1$. The approximation $Z = A_{\mathrm{O}}Z_{\mathrm{O}}$, Eq. (21) by use of Eq. (23) makes Eq. (87) reduce to:

$$\frac{\mathrm{d}\phi}{1-c\phi} = \frac{\hat{p}}{(Z_{\mathrm{O}})_\odot}\frac{\mathrm{d}s}{\mu_i} \quad , \quad (91a)$$

$$\phi = \frac{Z_{\mathrm{O}}}{(Z_{\mathrm{O}})_\odot} \quad , \quad c = \frac{(Z_{\mathrm{O}})_\odot}{\hat{p}}[A_{\mathrm{O}}\hat{p} + 1 - \zeta_{\mathrm{O}}] \quad , \quad (91b)$$

which can be integrated. After some algebra, the result is:

$$c\phi - c\phi_i = [1-c\phi_i]\left\{1 - \exp\left[-\frac{c\hat{p}}{(Z_{\mathrm{O}})_\odot}\frac{s-s_i}{\mu_i}\right]\right\} \quad , \quad (92)$$

where the index i denotes the starting configuration at the cosmic time t_i.

Reversing the role of the variables, Eq. (92) reads:

$$s - s_i = -\frac{(Z_{\mathrm{O}})_\odot\mu_i}{c\hat{p}}\ln\frac{1-c\phi}{1-c\phi_i} \quad , \quad (93)$$

which is monotonic in $c\phi$ within the domain $0 \le c\phi \le 1$.

Using the MacLaurin series expansion:

$$\exp\left[-\frac{c\hat{p}}{(Z_{\mathrm{O}})_\odot}\frac{s-s_i}{\mu_i}\right] = 1 - \frac{c\hat{p}}{(Z_{\mathrm{O}})_\odot}\frac{s-s_i}{\mu_i} + ..., \quad (94)$$

under the further assumption that the terms of order higher than the second can be neglected, Eq. (92) reduces to:

$$\phi - \phi_i = [1-c\phi_i]\frac{\hat{p}}{(Z_{\mathrm{O}})_\odot}\frac{s-s_i}{\mu_i} \quad , \quad (95)$$

$$\left|\frac{c\hat{p}}{(Z_{\mathrm{O}})_\odot}\frac{s-s_i}{\mu_i}\right| \le \left|(A_{\mathrm{O}}\hat{p} + 1 - \zeta_{\mathrm{O}})\frac{s_f - s_i}{\mu_i}\right| << 1 \quad , \quad (96)$$

where the index f denotes the ending configuration at the cosmic time t_f. If, in addition, $|c\phi_i| << 1$, Eq. (95) reduces to:

$$\phi - \phi_i = \frac{\hat{p}}{(Z_{\mathrm{O}})_\odot}\frac{s-s_i}{\mu_i} \quad , \quad (97)$$

which can be considered as the counterpart to the classical formulation, Eq. (29), in the special case of steady inflow regime $\kappa = -1$. The comparison between Eqs. (29) and (97), via (90), keeping in mind the star mass fraction s is linearly dependent on the cosmic time t in the case under discussion, shows the validity of Eq. (32).

A2 Dominant metal-free flow regime

The special case of dominant metal-free flow regime $|\kappa| >> 1$, $\zeta_{\mathrm{O}} = 0$ may be of particular relevance in connection with early stages of evolution, where the interstellar or intergalactic gas has still to undergo substantial metal enrichment, and deserves further analysis.

With regard to the parameter c appearing in Eq. (23), $|\kappa| >> 1$ implies $A_{\rm O}\hat{p} << |\kappa|$, as $\hat{p} << 1$ and $A_{\rm O}$ cannot significantly exceed unity via Eq. (21), being oxygen the most abundant metal in the universe. Accordingly, the following relations hold:

$$c = -\frac{(Z_{\rm O})_\odot}{\hat{p}}\kappa \quad , \qquad c\hat{p}'' = -\frac{(Z_{\rm O})_\odot \kappa}{1+\kappa} \quad , \qquad (98)$$

and Eqs. (24), (25), reduce to:

$$\phi - \phi_i = -\left[\frac{1}{(Z_{\rm O})_\odot}\frac{\hat{p}}{\kappa} + \phi_i\right] \times \times \left[1 - \left(\frac{\mu}{\mu_i}\right)^{-\kappa/(1+\kappa)}\right], \qquad (99)$$

$$\frac{\mu}{\mu_i} = \left[\frac{\hat{p} + (Z_{\rm O})_\odot \kappa\phi}{\hat{p} + (Z_{\rm O})_\odot \kappa\phi_i}\right]^{-(1+\kappa)/\kappa} \quad , \qquad (100)$$

where $-c\hat{p}''/(Z_{\rm O})_\odot$ is slightly exceeding or lowering the unity for inflowing ($\kappa < 0$) or outflowing ($\kappa > 0$) gas, respectively.

The power in μ/μ_i can be expanded in MacLaurin series as in Eq. (26), but the terms of the higher order with respect to the second can no longer be neglected via Eq. (28) due to $|\kappa| >> 1$ which implies $\mu_f >> \mu_i$ or $\mu_f << \mu_i$ depending whether $\kappa < 0$ or $\kappa > 0$, respectively.

In the limit $\kappa \to \infty$, $c\hat{p}''/(Z_{\rm O})_\odot \to -1$, Eqs. (99) and (100) reduce to:

$$\frac{\phi}{\phi_i} = \frac{\mu_i}{\mu} \quad , \qquad (101)$$

where normalized oxygen abundance is inversely proportional to the gas mass fraction, maintaining null if initially null.

ЈЕДНОСТАВАН ВИШЕФАЗНИ МОДЕЛ ЗАТВОРЕНА КУТИЈА + РЕЗЕРВОАР ХЕМИЈСКЕ ЕВОЛУЦИЈЕ

R. Caimmi

Dipartimento di Astronomia, Università di Padova
Vicolo Osservatorio 3/2, I-35122 Padova, Italy

E–mail: *roberto.caimmi@unipd.it*

УДК 524.6–54 : 524.3–52–54
Оригинални научни рад

У раду је унапређен модел хемијске еволуције тзв. модел затворене кутије и то на два начина: (i) уведен је једноставан модел затворена кутија + резервоар који допушта истицање гаса из кутије у резервоар (Hartwick 1976), као и прилив гаса из резервоара у кутију стопом која је пропорционална стопи формирања звезда (Caimmi 2007), и (ii) модел је проширен тако да може да обухвата више фаза (вишефазни модел затворена кутија + резервоар) током којих је стопа истицања или прилива гаса различита. Теоријски добијена расподела диференцијалне заступљености кисеоника блиска је непрекидној изломљеној линији. Модел је примењен на вештачки генерисан узорак сачињен од две групе хало-звезда, који по карактеристикама приближно одговара унутрашњем Галактичком халоу. Овако добијена емпиријска расподела диференцијалне заступљености кисеоника одговара, у значајној мери, непрекидној изломљеној линији за две одрживе емпиријске релације [O/H]-[Fe/H]. Одређени су нагиби и пресеци регресионих права, који су затим искоришћени као улазни параметри за вишефазни модел затворена кутија + резервоар. У границама грешака ($\mp\sigma$) нагиби регресионих права показују велики прилив гаса у раним фазама еволуције и слабо или умерено истицање гаса током каснијих фаза. Такође је разматрана и продискутована могућа веза унутрашњи хало – спољашњи овал (сиромашан металима). Квантитативни резултати не могу бити примењени на унутрашњи Галактички хало док се не уклоне контаминација диском и селекциони ефекти из узорака из халоа и не разреше неслагања добијена коришћењем различитих метода одређивања заступљености кисеоника.